

Contents lists available at ScienceDirect

Progress in Oceanography

journal homepage: www.elsevier.com/locate/pocean





Observation-based estimates of heat and freshwater exchanges from the subtropical North Atlantic to the Arctic

Feili Li ^{a,b,*}, M. Susan Lozier ^b, N. Penny Holliday ^c, William E. Johns ^d, Isabela A. Le Bras ^e, Ben I. Moat ^c, Stuart A. Cunningham ^f, M. Femke de Jong ^g

- ^a State Key Laboratory of Marine Environmental Science & College of Ocean and Earth Sciences, Xiamen University, Xiamen, China
- ^b School of Earth and Atmospheric Sciences, Georgia Institute of Technology, Atlanta, Georgia
- National Oceanography Centre, Southampton, UK
- d Rosenstiel School of Marine and Atmospheric Science, University of Miami, Miami, FL, United States
- e Woods Hole Oceanographic Institution, Woods Hole, MA, United States
- f Scottish Association for Marine Science, Oban, UK
- ⁸ Royal Netherlands Institute for Sea Research, Texel, the Netherlands

ARTICLE INFO

Kevwords:

Oceanic heat and salinity transports Surface heat and freshwater exchange Overturning and gyre circulation

ABSTRACT

Continuous measurements from the OSNAP (Overturning in the Subpolar North Atlantic Program) array yield the first estimates of trans-basin heat and salinity transports in the subpolar latitudes. For the period from August 2014 to May 2018, there is a poleward heat transport of 0.50 \pm 0.05 PW and a poleward salinity transport of 12.5 ± 1.0 Sv across the OSNAP section. Based on the mass and salt budget analyses, we estimate that a surface freshwater input of 0.36 \pm 0.05 Sv over the broad subpolar-Arctic region is needed to balance the ocean salinity change created by the OSNAP transports. The overturning circulation is largely responsible for setting these heat and salinity transports (and the derived surface freshwater input) derived from the OSNAP array, while the gyre (isopycnal) circulation contributes to a lesser, but still significant, extent. Despite its relatively weak overturning and heat transport, the Labrador Sea is a strong contributor to salinity and freshwater changes in the subpolar region. Combined with trans-basin transport estimates at other locations, we provide new estimates for the timemean surface heat and freshwater divergences over a wide domain of the Arctic-North Atlantic region to the north and south of the OSNAP line. Furthermore, we estimate the total heat and freshwater exchanges across the surface area of the extratropical North Atlantic between the OSNAP and the RAPID-MOCHA (RAPID Meridional Overturning Circulation and Heat-flux Array) arrays, by combining the cross-sectional transports with verticallyintegrated ocean heat and salinity content. Comparisons with the air-sea heat and freshwater fluxes from atmospheric reanalysis products show an overall consistency, yet with notable differences in the magnitudes during the observation time period.

1. Introduction

The ocean's role in the climate system stems from its ability to store and transport large amounts of heat (Rhein et al., 2014). Estimates of ocean heat content (OHC) change have revealed warming trends over the past few decades throughout the water column (Cheng et al., 2019; Cheng et al., 2017). Nowhere has this been more apparent than in the North Atlantic, where the most dramatic changes in OHC are found during the late 20th century (Zanna et al., 2019). Variability in the poleward oceanic heat transport (OHT) associated with the Atlantic meridional overturning circulation (AMOC) has been conjectured to

affect North Atlantic sea surface temperature (SST) and upper OHC (Bryden et al., 2020; Delworth; Zeng, 2016; Deser et al., 2010; Robson et al., 2016), mass loss from the Greenland Ice Sheet (GIS) (Holland et al., 2008; Rainsley et al., 2018; Straneo; Heimbach, 2013), and the decline of Arctic sea ice (Carmack et al., 2015; Polyakov et al., 2017; Polyakov et al., 2010).

The freshwater exchange also has important climate implications. Increased freshwater input (e.g., from the Arctic and GIS) to the subpolar North Atlantic has been posited to impact the formation of deep waters (Böning et al., 2016; Yang et al., 2016) and alter AMOC strength (Bakker et al., 2016; Haskins et al., 2020; Weijer et al., 2012). Evidence also

https://doi.org/10.1016/j.pocean.2021.102640

Received 22 November 2020; Received in revised form 15 June 2021; Accepted 30 June 2021 Available online 6 July 2021

0079-6611/© 2021 The Authors. Published by Elsevier Ltd. This is an open access article under the CC BY license (http://creativecommons.org/licenses/by/4.0/).

^{*} Corresponding author at: State Key Laboratory of Marine Environmental Science & College of Ocean and Earth Sciences, Xiamen University, Xiamen, China. E-mail address: feili.li@xmu.edu.cn (F. Li).

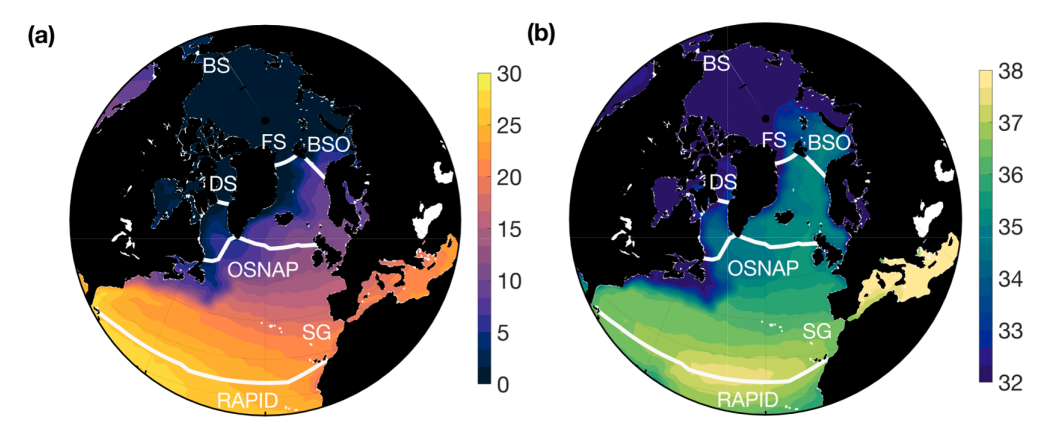


Fig. 1. Sea surface temperature and salinity over the Arctic–North Atlantic region. Color shading is (a) sea surface temperature (units: °C) and (b) salinity climatology from World Ocean Atlas 2018 (WOA18; 2005–2017 averages). White lines indicate the OSNAP and RAPID sections, along with main straits discussed in this analysis: BS – Bering Strait, DS – Davis Strait, FS – Fram Strait, BSO – Barents Sea Opening, SG – Strait of Gibraltar.

comes from paleo records from the last glacial cycle showing large and abrupt (over decades) AMOC shifts in response to the addition of freshwater in the region (see Lynch-Stieglitz, 2017, and references therein). The oceanic freshwater transport (OFT) across the northern or southern boundaries of the Atlantic is further suggested to be linked to the AMOC states (Jackson, 2013; Liu; Liu, 2012; Weijer et al., 2019).

More important than the OHT or OFT is the ocean heat or freshwater convergence/divergence for an enclosed basin, which induces changes in the ocean heat or salinity storage that can impact the basin-scale surface temperature and salinity patterns (Fig. 1). The latter are closely related to the air-sea heat and freshwater fluxes, which may influence the atmospheric circulation and provide potential feedbacks on the oceanic transports (e.g., Sutton et al., 2018). Understanding when and where the heat and freshwater transport change and how they affect the divergence is central to the coupled ocean–atmosphere system and to future climate predictions.

However, basin-wide measurements of the heat and freshwater (or salinity) transports are rare, especially in the subpolar region. Previous estimates of these transports have typically been based on quasisynoptic hydrographic sections along with direct ADCP (Acoustic Doppler Current Profiler) measurements (Holliday et al., 2018; Mercier et al., 2015; Rossby et al., 2017; Rossby et al., 2018) or derived velocity fields from inverse models (Fu et al., 2018; Ganachaud; Wunsch, 2003). In addition, there have been indirect estimates of OHT and OFT derived from sea level variations (Kelly et al., 2014; Kelly et al., 2016), and of OHT from the total atmospheric and oceanic energy budget (Trenberth; Caron, 2001; Trenberth; Fasullo, 2017; Trenberth et al., 2001; Trenberth et al., 2019).

Since 2014, a trans-basin observing system as part of the Overturning in the Subpolar North Atlantic Program (OSNAP; Lozier et al., 2017), has provided the first continuous measurements of full water column water properties and velocities in the subpolar region (Li et al., 2021; Lozier et al., 2019). The OSNAP array consists of two boundary-to-boundary segments: OSNAP West from Labrador to Greenland and OSNAP East from Greenland to the Scottish shelf. The OSNAP records have provided observational constraints of volume, heat and salinity transports in the region. They are key measurements as variations in these transports can cause property changes throughout the water columns and affect the ocean circulation. Data from OSNAP further provide an unprecedented opportunity to quantity the heat and freshwater divergence for the domains north and south of the OSNAP line, by combining the OSNAP transports with other boundary-to-boundary observations in the wider North Atlantic and Arctic region.

This work presents the 2014–2018 time series of the heat and salinity transports across the OSNAP section, followed by an examination of the heat and freshwater divergences over broad regions of the Arctic-

Atlantic north and south of the OSNAP line. The former uses historical estimates from Bering Strait, Davis Strait, Fram Strait, Barents Sea Opening, and the latter uses the RAPID Meridional Overturning Circulation and Heat-flux Array (RAPID-MOCHA or typically known as the RAPID array; Cunningham et al., 2007). Combined with observed ocean heat and salinity storage changes, the heat and freshwater exchanges across the surface area of subdomains are subsequently deduced through the heat and salt budgets. Finally, we compare surface heat and freshwater fluxes from atmospheric reanalyses with these new ocean observation-based estimates.

2. Data and methods

2.1. Data

We use continuous observations of volume, heat and salinity transports from two trans-Atlantic arrays: (a) Monthly estimates from April 2004 to August 2018 in the subtropics from the subtropical RAPID array (Johns et al., 2011; McDonagh et al., 2015; Moat et al., 2020), and (b) 30-day estimates from August 2014 to May 2018 from the subpolar OSNAP array (https://doi.org/10.35090/8hqw-c147). Both the RAPID and OSNAP transport fields use International Thermodynamic Equation of Seawater-2010 (TEOS-10, IOC et al., 2010; McDougall; Barker 2011) in the transport estimates, e.g., for the geostrophic calculations from the dynamic height moorings.

Monthly gridded temperature and salinity datasets are used to derive the changes in the OHC and the ocean salt content (OSC), which include: (a) UK Met Office Hadley Centre Enhanced Ocean Data Assimilation and Climate Prediction (ENACT) archive version4 dataset (EN4, Good et al., 2013) between January 2004 and December 2018 (http://www. metoffice.gov.uk/hadobs/en4), (b) International Pacific Research Center (IPRC) gridded Argo products between January 2005 and December 2018 (http://apdrc.soest.hawaii.edu/projects/Argo/data/gridded), (c) Copernicus Marine Environment Monitoring Service (CMEMS) Gridded CORA-In-Situ Observations Objective Analysis in Delayed Mode (Gaillard et al., 2016) between January 2004 and December 2018 (https://marine.copernicus.eu/), and (d) CMEMS Multi-observation Global Ocean ARMOR-3D Level 4 Analysis (Guinehut et al., 2012; Mulet et al., 2012) between January 2004 and December 2018 (https://marine.copernicus.eu/). More details on these datasets are summarized in Table S1.

Monthly atmospheric air-sea heat and freshwater flux datasets are from: (a) National Centers for Environmental Prediction Climate Forecast System version 2 (NCEP CFSv2, Saha et al., 2014) for January 2011 to December 2018 (https://doi.org/10.5065/D69021ZF), (b) the Japanese 55-year Reanalysis (JRA55, Harada et al., 2016; Kobayashi et al.,

Table 1

Heat or temperature transport across the trans-basin sections, and the derived surface heat exchange Q_{sfc} for the enclosed ocean basins within the broader-Arctic region. All values are the time-mean plus/minus uncertainty. The uncertainty in the mean OSNAP transports includes the standard error in the 4-year mean transport (0.01, 0.01 and 0.004 PW for the full OSNAP array, OSNAP East and West, respectively) and a bias error that accounts for any possible biases in the observing system (0.04, 0.04 and 0 PW for the full OSNAP array, OSNAP East and West, respectively, Li et al., 2017). The uncertainty in Q_{sfc} is derived by combining the uncertainty in individual oceanic transports. Positive (negative) values indicate heat sources (sinks) for the respective ocean basin.

| | OSNAP | Bering Strait | Q_{sfc} | OSNAP West | Davis Strait | Q_{sfc} | OSNAP East | Fram Strait | Barents Sea Opening | $Q_{ m sfc}$ |
|--------------|----------------|-----------------------|------------------|---------------|---------------------------------|--------------------|---------------|----------------------------|------------------------|------------------|
| Heat (PW) | 0.50 ± 0.05 | 0.012 ± 0.001^{a} | -0.51 ± 0.05 | 0.079 ± 0.004 | $^{-0.030~\pm}_{0.006^{\rm b}}$ | -0.049 ± 0.007 | 0.43 ± 0.05 | $-0.036 \pm 0.006^{\circ}$ | -0.072^{d} | -0.32 ± 0.05 |

 $^{^{\}rm a}$ 2003-2015 mean, referenced to freezing temperature $-1.9~^{\circ}\text{C}$ (Woodgate, 2018).

2015) for January 2004 to December 2018 (https://jra.kishou.go.jp/JRA-55/index_en.html#download), and (c) Fifth generation of the European Centre for Medium-Range Weather Forecasts (ECMWF) atmospheric reanalyses (ERA5, C.C.C.S., 2017) for January 2004 to December 2018 (https://cds.climate.copernicus.eu/cdsapp#!/home). Details on atmospheric reanalyses are in Table S2. Air-sea heat flux was calculated as the sum of latent, sensible, shortwave and longwave heat fluxes. Freshwater flux was a combination of evaporation, precipitation, and water run-off.

2.2. Calculations of heat, salinity transports and surface freshwater exchange

Oceanic heat and salinity transports The OHT is defined as,

$$OHT = \iint \rho C_P v \theta dx dz, \tag{1}$$

where v is velocity normal to the trans-basin section, ρ is water density, $C_P = 4000Jkg^{-1}K^{-1}$ is the specific heat capacity of water, θ is potential temperature of water, and the double integral is taken over the full area of the section (x and z are horizontal and vertical coordinates, respectively). Only when the net mass flux is zero, Eq. (1) yields a true heat transport that is independent of any reference temperature. Otherwise, it gives a temperature transport relative to 0 °C.

The oceanic salinity transport (OST) is defined as,

$$OST = \iint vSdxdz,$$
(2)

where *S* is sea water salinity on the practical salinity scale (PSS-78). Note that there are no formal units for salinity on this scale and thus the unit of OST is Sv. This is equivalent to the traditionally used Sv psu (practical salinity unit).

The OHT and OST are derived from the cross-sectional velocity, potential temperature, salinity data at individual sections.

Surface heat exchange

Heat exchange across the surface area of an ocean basin, Q_{sfc} , can be estimated as,

$$Q_{sfc} = Q_{adv} + Q_{OHC}, (3)$$

where

$$Q_{adv} = -\iint \rho C_P v \theta dx dz, \tag{4}$$

$$Q_{OHC} = \frac{dOHC}{dt} = \frac{d}{dt} \iiint \rho C_P \theta dV.$$
 (5)

In Eqs. (4) and (5), ν is inwards-positive velocity normal to the

boundary of the basin, and the integral follows the complete circuit of the boundary, V is the total volume of water in the basin. Q_{adv} is the airsea heat exchange required to compensate any OHT at the ocean boundary. For example, a negative Q_{adv} (heat loss to the atmosphere through the sea surface) is needed to account for a positive OHT (heat gain into the basin at the boundary). Q_{OHC} is associated with the change in the OHC, and its relationship with Q_{sfc} is straightforward. A negative Q_{sfc} (heat loss) is required to account for a cooling basin (decreasing OHC). Note that the diffusive term has been neglected due to its negligible effect on the heat divergence over the time scales of interests. In addition, using a constant C_P has no appreciable effect on the results.

In this study, Q_{OHC} estimates are derived from the ensemble mean of four gridded temperature products, and their uncertainty is derived based on typical measurement errors and differences between the individual products (Appendix B).

Surface freshwater exchange

There is a relationship between ocean salinity and freshwater, where salinity changes are related to the addition (or removal) of freshwater to (or from) the ocean (e.g., Aagaard; Carmack, 1989). It allows for an indirect way to estimate the freshwater input across the ocean surface in terms of oceanic salinity transports. Such an approach is based on the conservation of mass and salt within a fixed volume of ocean, so that freshwater added to (removed from) the ocean through its surface is accounted by the net salinity transport across the boundary and changes in the OSC itself (e.g., Bacon et al. (2015); Ganachaud; Wunsch, 2003; Tsubouchi et al., 2012). This approach yields a true freshwater transport across the ocean surface that depends on advective salt flux divergence. It thus avoids the problems associated with arbitrary reference salinities that can lead to an ambiguous estimate of freshwater transport (Schauer; Losch, 2019).

The freshwater exchange across the surface area of an ocean basin (i. e., precipitation, evaporation, river runoff, ice melt), FW_{sfc} , can be estimated as,

$$FW_{sfc} = FW_{adv} + FW_{OSC}, (6)$$

where

$$FW_{adv} = \frac{1}{\overline{S}} \iint S' v' dx dz, \tag{7}$$

$$FW_{OSC} = -\frac{1}{\overline{S}} \left[\frac{\partial}{\partial t} \iiint SdV \right]$$
 (8)

In Eqs. (6)–(8), \overline{S} is the boundary-mean salinity averaged over the whole boundaries of the basin, and S are deviations from the mean. Similarly, v are deviations from the boundary-mean velocity. By construction, integrating v and S along the whole boundary yields zero. FW_{adv} accounts for the salinity change induced by the volume and salinity transports across the boundary. For example, if inward-flowing

^b 2004-2006 mean, averaged of the 2004–2005 temperature transport of 0.02 ± 0.009 PW into the Arctic (referenced to 0 °C) (Curry et al., 2011) and the 2005–2006 temperature transport of 0.04 ± 0.009 PW into the Arctic (referenced to 1 °C) (Tsubouchi et al., 2018).

^c 1997-2009 mean, derived from closed volume budget (Schauer; Beszczynska-Moller, 2009).

d 1997-2009 mean, referenced to 0 °C; sum of the temperature transport of 0.050 PW for the Atlantic Water and 0.034 PW for the Norwegian Coastal Current both into the Barents Sea, and 0.012 PW for the Bear Island Trench out of the Barents Sea (Skagseth et al., 2008; Smedsrud et al., 2010).

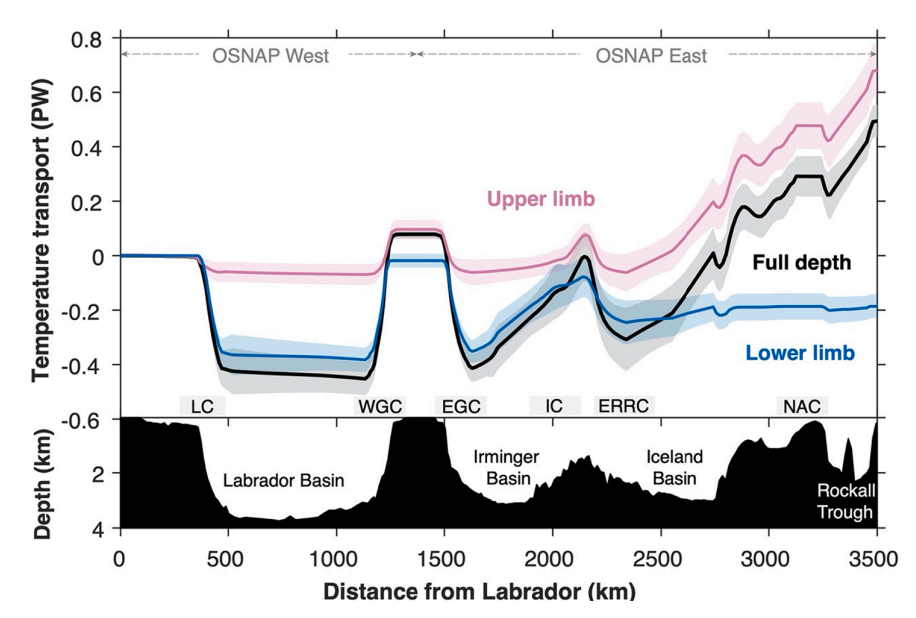


Fig. 2. August 2014–May 2018 mean temperature transport accumulated eastward along the OSNAP array for the full water column, and the upper and lower AMOC limbs that is delimited by the isopycnal 27.65 kg m⁻³. Only when the full-depth integrated temperature transport is summed over the whole section (the rightmost point of the black line), it represents a meaningful heat transport. Positive transport is poleward. Shading indicates one standard deviation from all 30-day estimates. Major currents are labeled at the top of the bathymetry: LC – Labrador Current, WGC – West Greenland Current, EGC – East Greenland Current, IC – Irminger Current, ERRC – East Reykjanes Ridge Current, NAC – North Atlantic Current.

waters are more saline than outward-flowing waters at the boundary, a positive FW_{adv} (an addition of freshwater) is required to account for the salinity increase. FW_{OSC} is associated with the change in the OSC in the basin. That is, a positive FW_{OSC} (an addition of freshwater) is required for a freshening basin (decreasing S). The reader is referred to Appendix A for the full derivations. Similar to the OHC changes, FW_{OSC} is derived as the ensemble mean based on four gridded salinity products (Appendix B). Finally, we note that the diffusive term has been neglected due to its negligible effect on the salt divergence over the time scales of interests.

 FW_{sfc} may be considered as an equivalent OFT through the boundary section that compensates FW_{sfc} at each time step. That is, a positive FW_{sfc} (freshwater added to the basin at the surface) can be thought of as a negative OFT (freshwater exported from the basin across the boundary). This equivalence provides a practical way for comparing FW_{sfc} estimates with historical OFT estimates. Because earlier OFT estimates typically used an arbitrary choice of reference salinity (Schauer; Losch (2019)), these estimates would need to be recalculated using the corresponding boundary-mean salinity before they could be appropriately compared to FW_{sfc} . Unless otherwise specified, the freshwater transport estimates in the subsequent analysis represent FW_{sfc} , not OFT.

3. Results

3.1. Subpolar heat transport across OSNAP

The 2014-2018 mean heat transport across the OSNAP line is 0.50 ± 0.05 PW (Table 1). This is a true heat transport because of a zero-net-throughflow constraint across the full section (Lozier et al., 2019). We note that the application of such a constraint is typically required for determining the missing barotropic component of the flow fields at the boundary-to-boundary section (e.g., McCarthy et al., 2015; Lozier et al., 2019). Due to a small magnitude of the throughflow (~1 Sv), its omission has no impact on the total transport estimates (up to \sim 0.01 PW). The poleward heat transport across OSNAP is associated with the cooling of warm Atlantic waters (~10 °C) to the colder North Atlantic Deep Water (NADW; <4 °C), which essentially constitute the upper and lower limbs of the AMOC in the region (Fig. S1). The upper limb temperature transport is concentrated in the eastern part of the section in the eastern Iceland basin and the Rockall Trough through main branches of the North Atlantic Current (NAC; Fig. 2). The temperature transport carried in the lower limb is accomplished by deep

boundary currents carrying the NADW in the Labrador, Irminger and Iceland basins. Those boundary currents move both poleward and equatorward across the OSNAP array, showing considerable spatial variations. In total, the subpolar heat transport is a residual between the poleward temperature transport of 0.69 PW in the AMOC upper limb (with a volume transport of 16.6 Sv, Li et al., 2021) and the equatorward transport of 0.19 PW in the lower limb.

The temperature transports vary geographically in different basins and in association with major boundary currents. Overall, the mean subpolar heat transport is mostly (86%) contained at OSNAP East in the eastern subpolar basin (0.43 PW) with a small fraction at OSNAP West in the Labrador basin (0.079 PW). We note that for the OSNAP West and East segments separately, it is a temperature transport relative to 0 °C because the mass flux is not zero across the section (net volume transport of 1.6 Sy equatorward across OSNAP West while 1.6 Sy poleward across OSNAP East, Lozier et al., 2019). The main branches of the NAC carry a poleward temperature transport, with about 0.5 PW through the eastern Iceland basin and 0.3 PW through the Rockall Trough (black line, Fig. 2; see Table S3 for more information on the associated volume and temperature transports). West of the NAC, the circulation across the western Iceland basin, and the Irminger and Labrador basins contributes to an equatorward temperature transport of 0.3 PW. We have estimated the transport associated with other main boundary currents intercepted by the OSNAP boundary arrays. In the mean, there is a temperature transport of -0.3 PW carried by the East Reykjanes Ridge Current (ERRC) in the western Iceland basin, 0.1 PW by the Irminger Current (IC) in the eastern Irminger basin, and $-0.5 \ PW$ by the East Greenland Current (EGC) in the western Irminger basin. Within the Labrador Sea, there is a temperature transport of 0.5 PW in the West Greenland Current (WGC) and -0.4 PW in the Labrador Current (LC).

The total heat transport across OSNAP exhibits substantial month-tomonth variations throughout the 2014–2018 time period, with a range of \sim 0.4–0.6 PW (Fig. 3a). The record shows a weak seasonal cycle, and a longer time series will be needed to fully evaluate its seasonality. The heat transport can be broken down to components that are associated with the throughflow, and overturning and gyre (isopycnal) circulations, which describe the heat transport accomplished by the net volume transport (throughflow), zonally-averaged circulation along density surfaces (overturning component) and the deviation of velocity and temperature from these zonal averages (isopycnal component) (Lozier et al., 2019). Fig. 3a shows that the overturning component dominates

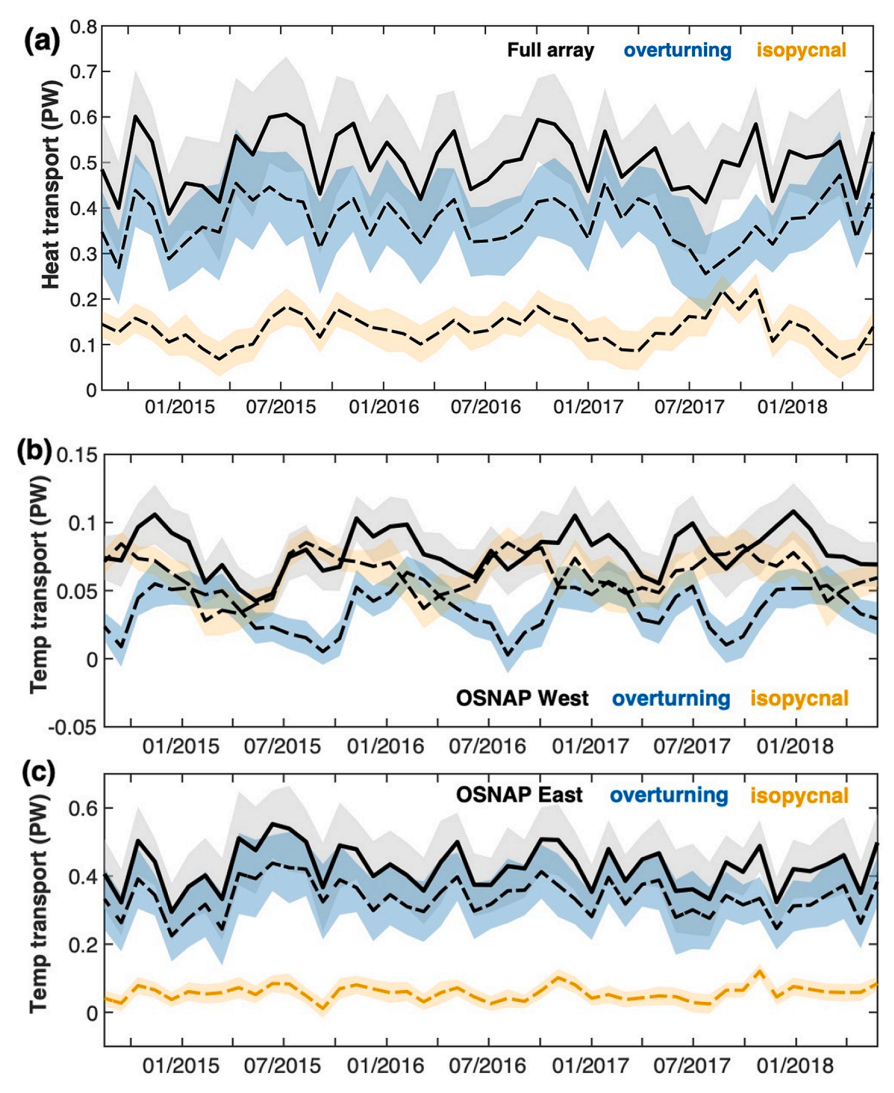


Fig. 3. Time series of the heat transport across the (a) full OSNAP array, and the temperature transport relative to 0 °C across (b) OSNAP West and (c) East. Also shown are the overturning and isopycnal components. Positive transport is poleward. Shading indicates the uncertainty for each monthly estimate obtained via the Monte Carlo simulations (Lozier et al., 2019). Note that the y-axis ranges are different.

the subpolar heat transport, which accounts for 74% of the mean (Table S4) and 68% of the total variance. It suggests a significant contribution from the isopycnal component especially in the total subpolar transport variability. The main characteristics of the subpolar heat transport are consistent with the earlier publication using the first 21-month OSNAP record (Lozier et al., 2019).

Applying the same decomposition across OSNAP West and East reveals distinct features in the two sections. The overturning component dominates the temperature transport across OSNAP East (Fig. 3 and Table S4): it accounts for 79% of the mean and 90% of the total variance. Conversely, the temperature transport across OSNAP West in the Labrador basin is mostly carried by the isopycnal component, which accounts for 78% of the mean. This is consistent with earlier studies showing the dominance of the horizontal circulation in the temperature transport in the Labrador basin (Pickart; Spall, 2007; Straneo, 2006). However, the isopycnal or overturning component alone can only explain 19% and 36% of the variance in the Labrador basin temperature transport, respectively. This is due to a general anti-correlation of the seasonal cycles of the overturning and isopycnal heat transports (correlation coefficient is -0.45 at zero lag; statistically significant at the

95% level). The seasonality in the overturning component is associated with the seasonal variation in the strength of the overturning circulation (Holte; Straneo 2017; Li et al., 2021), which has its maximum in winterspring. The seasonality in the isopycnal component has similar amplitudes with maximum in fall through early winter, which arises mainly from the variations in the transport of warm Irminger Water in the WGC (Pacini et al., 2020).

3.2. Heat transport divergence between OSNAP and Bering Strait

The heat transport divergence north of the OSNAP line can be derived from the heat/temperature transport across the OSNAP sections together with historical estimates of the temperature transports across the main straits of the Arctic Ocean. To be specific, we examine the heat divergence in the broader-Arctic basin enclosed by the Bering Strait and the complete OSNAP section, and additionally in two subarctic-subpolar basins west and east of Greenland, respectively: one is enclosed by the Davis Strait and OSNAP West, and the other is by the Fram Strait-Barents Sea Opening and OSNAP East (Fig. 1). Note that the transport estimate at different locations represents the mean condition over the respective

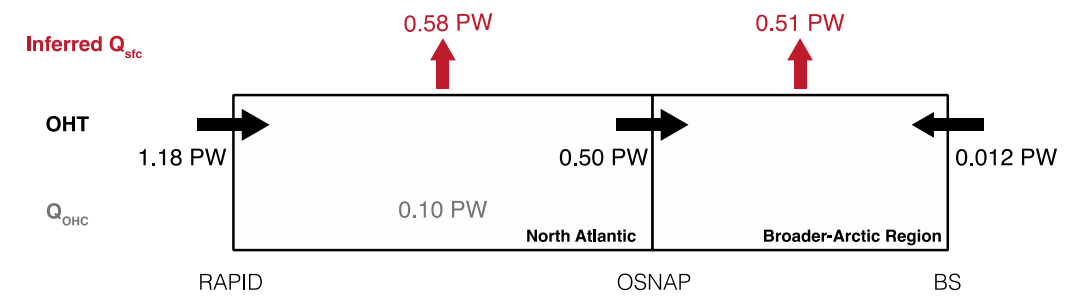


Fig. 4. Heat budget for the ocean basin between the Bering Strait (BS) and OSNAP, and between OSNAP and RAPID. Black (red) arrows indicate the direction of the heat or temperature transports (or surface exchanges). For the change in the OHC, a positive value indicates a heat accumulation for the domain. Values for OSNAP and RAPID are derived from 2014 to 2018 observations, while it is the 2003–2015 mean estimate for BS (Tables 1 and 2). (For interpretation of the references to color in this figure legend, the reader is referred to the web version of this article.)

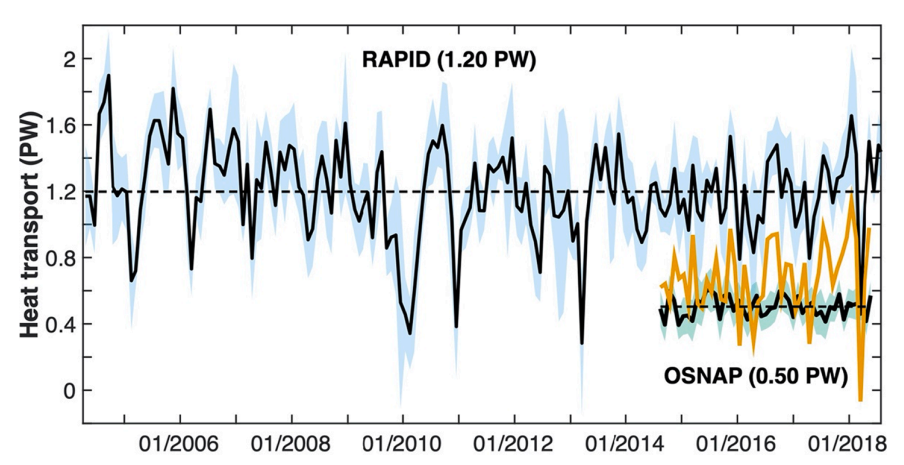


Fig. 5. Monthly time series of the heat transport at OSNAP and RAPID (black lines; shading for uncertainty) and the resultant heat transport divergence between the two lines (yellow line). Positive transport is poleward; positive divergence represents a heat convergence for the extratropical basin between OSNAP and RAPID. Numbers in parenthesis are the time-mean heat transport averaged over the whole length of respective record (dashed lines). (For interpretation of the references to color in this figure legend, the reader is referred to the web version of this article.)

time period (Table 1).

The results indicate an overall heat convergence of 0.51 PW in the broader-Arctic domain between the Bering Strait and OSNAP. In the absence of any net heat storage over this domain, this implies a net heat loss form the ocean to the atmosphere of 0.51 PW over this region (Fig. 4), which we denote as Q_{sfc} . Similarly, we estimate a surface heat loss of 0.049 PW over the Labrador Sea between the Davis Strait and OSNAP West, and 0.32 PW over the region east of Greenland between the Fram Strait-Barents Sea Opening and OSNAP East. The dominance of the heat loss over the subarctic-subpolar basins north of OSNAP East is consistent with the characteristics of water mass transformation at high latitudes (Desbruyeres et al., 2019). In addition, the net heat loss east of Greenland is nearly the same (0.16 PW) north and south of the Greenland-Scotland Ridge if we take into account the poleward heat transport of 0.26 PW across the Ridge (Rossby et al., 2018).

The results provide important observational constraints for the airsea heat exchanges, which have been shown to be underestimated significantly in the eastern subpolar region by atmospheric reanalyses (by $\sim 50\%$, Chafik; Rossby, 2019). Uncertainty in our estimates remains due to the different time periods covered by the observations at OSNAP and other locations. Specifically, the temperature transport estimates across the Bering Strait, Fram Strait and Barents Sea Opening are representative of the 2000s' mean condition, while the estimate at Davis Strait represents 2004–2006 conditions and the OSNAP estimate represents the 2014–2018 condition (see Table 1). However, previous modeling studies suggest a weak decadal variability in the temperature transport across the Arctic straits (typical of ~ 0.005 PW, Ilicak et al., 2016). The OSNAP transports appear to dominate the heat transport divergences (both mean and variability) in the domain north of the section. This is likely the same prior to the OSNAP observations. As such,

the contemporary and continuous OSNAP measurements across the entire subpolar basin offer best estimates of the heat divergences in respective subdomains during the 2014–2018 time period. Longer OSNAP records will be needed to evaluate the robustness of the observational estimates on longer time scales. Finally, the temperature transports at the Arctic straits are calculated from different methods, e. g., with different reference temperatures, which however cause only a negligible impact on the transport estimate due to the relatively small volume transport at each strait (typically $\sim 1{\text -}2$ Sv).

3.3. Heat budget between OSNAP and RAPID

The total surface heat exchange Q_{sfc} over the North Atlantic basin south of the OSNAP line can be derived by taking into account the OHT across the bounding OSNAP and RAPID sections (Q_{adv}), and the OHC change within the domain (Q_{OHC}).

3.3.1. Oceanic heat transport and divergence

The Atlantic Ocean's heat transport is known to be strongest in the subtropical North Atlantic (Ganachaud; Wunsch, 2000; Trenberth et al., 2001). The 2004–2018 mean heat transport across RAPID at $26^{\circ}N$ is 1.20 ± 0.10 PW. The corresponding heat transport across the RAPID line for the 2014–2018 period that is in common with the OSNAP observations is 1.18 ± 0.13 PW. A slight increase in the uncertainty is due to the shorter temporal coverage.

Comparisons of the RAPID and OSNAP estimates reveal several contrasting features of the subtropical and subpolar heat transports (Fig. 5). First, the subtropical heat transport is more variable over monthly to interannual time scales. The poleward heat transport at RAPID is more than twice as large as that observed at OSNAP and its

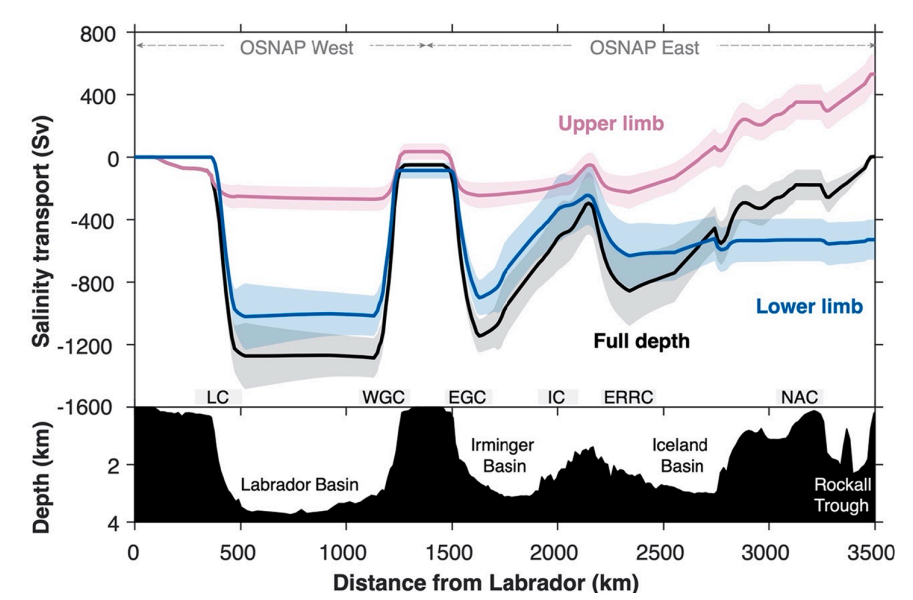


Fig. 6. August 2014–May 2018 mean salinity transport accumulated eastward along the OSNAP array for the full water column, and the upper and lower AMOC limbs that is delimited by the isopycnal 27.65 kg m⁻³. Positive transport is poleward. Shading indicates one standard deviation from all 30-day estimates. Major currents are labelled at top of the bathymetry: LC – Labrador Current, WGC – West Greenland Current, EGC – East Greenland Current, IC – Irminger Current, ERRC – East Reykjanes Ridge Current, NAC – North Atlantic Current.

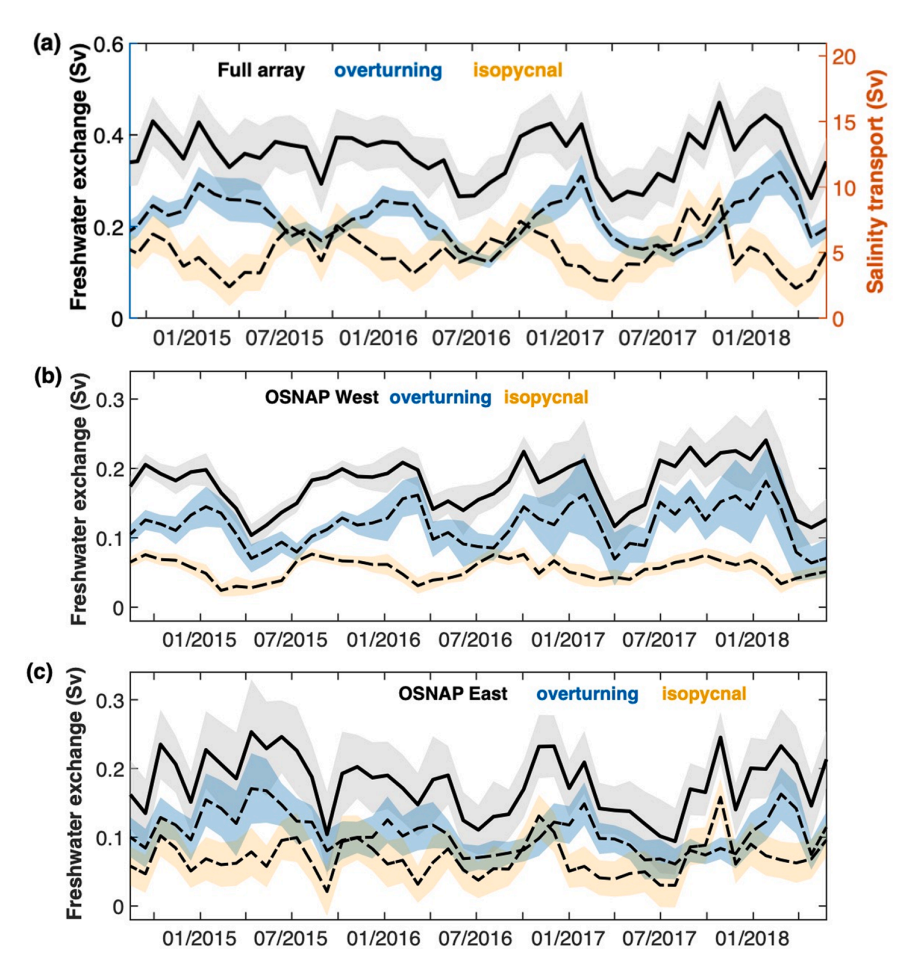


Fig. 7. Time series of the surface freshwater exchange for the region between the Bering Strait and the OSNAP line, derived from (a) the full OSNAP array, (b) OSNAP West and (c) East, along with the overturning and isopycnal components. The magnitudes of the OSNAP salinity transport and its overturning and isopycnal components are indicated by the right y-axis in (a). Positive freshwater exchange indicates a freshwater addition to the ocean, and positive salinity transport is poleward across the section. Shading indicates the uncertainty in each monthly estimate obtained via the Monte Carlo simulations (Lozier et al., 2019). Note that the left y-axis ranges are different for (a) and for (b)(c).

monthly standard deviation (0.28 PW) is ~ 5 times as large as that at OSNAP (0.05 PW). Second, the overturning circulation accounts for more than 90% of the heat transport in the subtropics in terms of both its

mean and variance (see Johns et al., 2011; McCarthy et al., 2015), while in the subpolar gyre the overturning component, though still dominant, explains about 70% of the mean and variance. Thus, the isopycnal

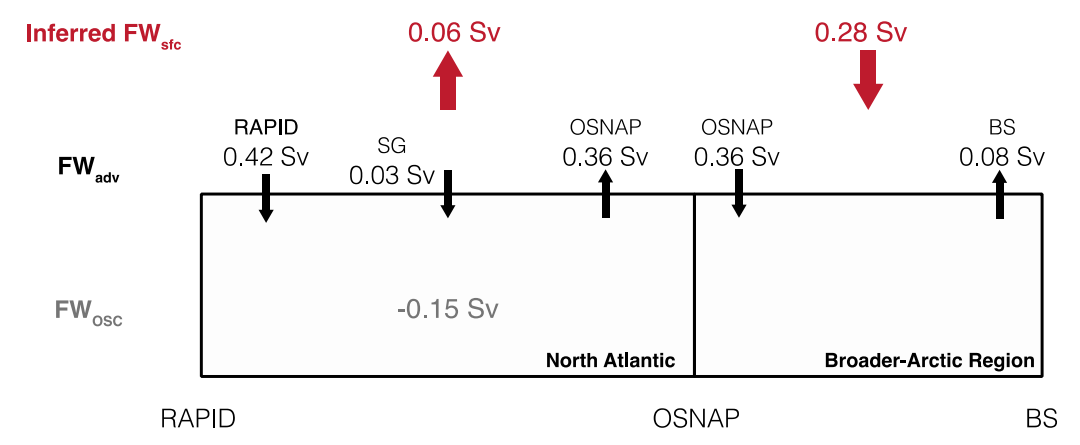


Fig. 8. Freshwater budget for the ocean basins between the Bering Strait (BS) and OSNAP, and between OSNAP and RAPID. Arrows indicate the direction of the surface freshwater exchange. For the FW_{OSC}, a negative value indicates a freshwater removal from the ocean (increasing salinity). The surface freshwater exchange related to the oceanic volume and salinity transports across RAPID, the Strait of Gibraltar (SG), OSNAP and BS are indicated by the black arrows. Values for OSNAP and RAPID are obtained from 2014 to 2018 observations; those for BS and SG are estimates of the long-term means (Tables 3 and 4). Note that the net poleward salinity transport across OSNAP causes opposing surface freshwater exchange for the basins north and south of the section.

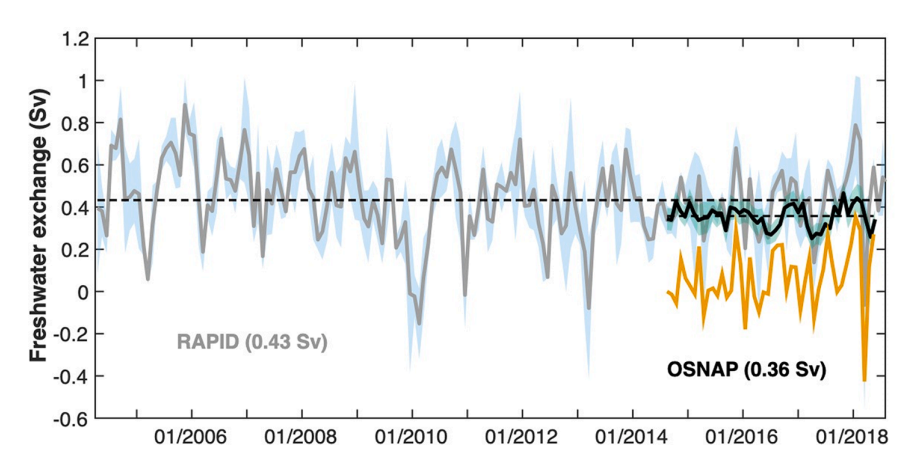


Fig. 9. Monthly time series of the surface freshwater exchange derived from OSNAP and RAPID (black and gray lines; shading for uncertainty) over the region bounded by the Bering Strait and respective section. Numbers in parenthesis are the time-mean estimates averaged over the whole length of respective record (dashed lines). The yellow line indicates the resultant surface freshwater convergence over the region. Positive (negative) values indicate freshwater sources (sinks) for the ocean. (For interpretation of the references to color in this figure legend, the reader is referred to the web version of this article.)

Table 2

Extratropical North Atlantic heat budget (units: PW). The numbers are de-seasonalized time-mean plus/minus uncertainty. The observation-based Q_{sfc} estimate is obtained as the sum of Q_{adv} and Q_{OHC} . Q_{sfc} derived from the atmospheric reanalysis products are included for comparisons. The uncertainty in the RAPID heat transport includes the standard error of the time-mean heat transport (0.06 PW for 2014–2018, 0.03 PW for 2004–2018) and a possible bias error in the estimate (0.07 PW, Johns et al., 2011). Q_{OHC} is derived from gridded temperature datasets (Appendix B). The uncertainty in Q_{adv} and in the observation-based Q_{sfc} are derived by combining the component errors in quadrature. The uncertainty in those atmospheric reanalyses only contain the standard error of the mean estimate, which is derived from the deseasonalized values to exclude the large (quasi-deterministic) variance associated with the seasonal cycle of the surface fluxes. Positive (negative) values indicate heat sources (sinks) for the enclosed basin.

| | OSNAP | RAPID | Q_{adv} | Q_{OHC} | Q_{sfc} | | | |
|---------------|-------------------------------|-----------------|----------------|---------------|----------------|--------------------|----------------|----------------|
| | | | | | Observation | NCEP CFSv2 | JRA55 | ERA5 |
| 8/2014-5/2018 | -0.50 ± 0.05 | 1.18 ± 0.13 | -0.68 ± 0.14 | 0.10 ± 0.07 | -0.58 ± 0.16 | -0.48 ± 0.03 | -0.79 ± 0.03 | -0.47 ± 0.03 |
| 4/2004-8/2018 | -0.50 ± 0.07 ^a | 1.20 ± 0.10 | -0.70 ± 0.12 | 0.03 ± 0.02 | -0.67 ± 0.12 | -0.46 ± 0.02^{b} | -0.80 ± 0.01 | -0.49 ± 0.01 |

a Data available for August 2014–May 2018. Note that we add 0.02 PW to the uncertainty estimate to account for possible errors over longer periods.

component of the heat transport is relatively more important in the subpolar gyre, and has a value (0.13 PW) comparable to that at RAPID (0.10 PW), despite the overall heat transport at RAPID being more than two times larger than at OSNAP. Third, there is a stronger linear dependence of the heat transport on the strength of the overturning circulation in the subtropics (0.08 PW/Sv at RAPID) than that in the subpolar region (0.01 PW/Sv at OSNAP, Fig. S2). This is related to a greater temperature gradient between the AMOC's upper and lower

limbs in the subtropics, and in particular to its much warmer upper limb (as shown in the sea surface temperature in Fig. 1), as well as a stronger contribution from overturning to the total heat transport in the subtropics.

Combining the OSNAP and RAPID estimates reveals a convergence of OHT in the extratropical North Atlantic basin between these lines, which is $0.68\ \pm\ 0.14$ PW during the overlapping time period for 2014–2018. We include this as a heat transport divergence in the surface heat budget

b Data available for January 2011–August 2018.

 $(Q_{adv} = -0.68 \mathrm{PW}, \mathrm{Table~2})$. The temporal variability in Q_{adv} is dominated by the RAPID heat transport variability in the subtropics, e.g., both showing a clear seasonal cycle with the maximum in summer (July-August) and minimum in early spring (March-April; Fig. S3).

3.3.2. Surface heat exchange

The OHC changes in the ocean basin between OSNAP and RAPID correspond to a heat gain during the 2014–2018 period (Appendix B; Fig. B.1). The derived Q_{OHC} exhibits a strong seasonality ($\sim\pm3$ PW, Fig. S3) as well as large interannual variations ($\sim\pm1$ PW, Fig. S4).

The seasonality may introduce a bias in the time-mean estimate when different parts of the year are sampled unevenly. This is especially the case for a short time series of a few years; for example, the OSNAP record is 3.8 years long, with June and July being sampled in only 3 of the 4 years. To account for this, we constructed a composite monthly climatology by averaging all data from the same months, from which we draw a 'de-seasonalized' estimate of the time-mean transports, and use this to estimate all time-mean heat transports.

During 2014–2018, there was a warming over the region between the RAPID and OSNAP sections at the rate of 0.10 PW. Combining this with the time-mean Q_{adv} of -0.68 PW then gives the mean Q_{sfc} of -0.58 PW for 2014–2018, indicating a net heat loss to the atmosphere from the extratropical North Atlantic (Table 2 and Fig. 4).

3.3.3. Comparison with atmospheric reanalyses

The observation-based Q_{sfc} estimates are compared to those derived from atmospheric reanalysis products (NCEP CFSv2, JRA55, and ERA5). These reanalysis products including earlier versions have been used widely in studying the surface-forced water mass transformation and overturning in the North Atlantic (e.g., Desbruyeres et al., 2019; Grist et al., 2014). The net air-sea heat fluxes from reanalyses have been integrated over the surface area of the extratropical North Atlantic basin between the OSNAP and RAPID lines $(1.9 \times 10^{13} m^2)$ to derive the net surface heat exchange in PW.

All three products show consistently a heat loss from the ocean to the atmosphere, with similar seasonal and interannual variability (Figs. S3) and S4). When not considering the shared seasonality, there is only a weak correlation between the observation-based estimates and the reanalysis products that is not statistically significant. The time-mean estimates based on reanalyses are different from each other and all depart from our estimate from oceanic observations (Table 2). JRA55 (-0.79 PW) exhibits the strongest surface heat loss, which is $\sim 60\%$ stronger than NCEP CFSv2 (-0.48 PW) and ERA5 (-0.47 PW). The uncertainty in these reanalyses (0.03 PW) only contain the standard error in the mean estimate, and does not include any bias errors, because this type of error is not well known for the reanalysis products. Alternatively, the size of potential bias errors in Q_{sfc} for the atmospheric reanalysis products may be estimated by comparing their mean values to our observationally-derived estimates. For the 2014-2018 period, the results show that Q_{sfc} from JRA55 is stronger than the observations by 0.21 PW (or 36%), where the difference is statistically significant at the 1σ level (67%) according to the error bars. NCEP CFSv2 and ERA5 have comparable heat loss that is 0.10-0.11 PW (or 18%) weaker than the observed value. However, such differences are not statistically significant even at the 1σ level. None of the observation-reanalysis differences are significant at the 2σ level (95%).

To put our estimates in a climatological context, we next extend the heat budget analysis for the whole length of the RAPID record from April 2004 to August 2018 (Table 2). Of note are the limited length of the record: (i) For the OSNAP data, the mean estimate is from the 4-year long record. We note that the variability in the ocean heat transport divergence during 2014–2018 is governed by variability at RAPID and the same likely holds before 2014. In addition, decadal changes in the subpolar heat transports are generally weak during the past few decades (~0.01–0.02 PW, Li et al., 2017; Rossby et al., 2017), which can be

thought of as an additional error in the longer-term transport estimate (see Table 2). (ii) For NCEP CFSv2, the mean estimate is based on the available record between January 2011 and January 2017 (73 months).

The observation-derived $Q_{\rm sfc}$ is -0.67 PW during 2004–2018, which is a 16% stronger surface heat loss than the 2014–2018 time period. The intensification is mainly related to a reduced rate of net warming of the North Atlantic for the 2004–2018 period: the region between the RAPID and OSNAP lines warmed at a rate of only 0.03 PW during 2004–2018 compared to 0.10 PW that during 2014–2018. This highlights an accelerated warming during the most recent years in the broad subpolar-subtropical region, despite the strong cooling occurred in the subpolar gyre during 2013–2015 (Josey et al., 2018) which was overcome by the warming in the subtropics. By comparison, there was only a marginal strengthening in the oceanic heat transport across RAPID during 2004–2018.

There are slight Q_{sfc} changes (\sim 0.01–0.02 PW) in the reanalysis products for the longer 2004–2018 time period. Comparisons with the observations indicate a reduced (increased) discrepancy for JRA55 (NCEP CFSv2 and ERA5) with the longer records. For the 2004–2018 means, JRA55 Q_{sfc} is 0.13 PW (or 19%) stronger than the observational estimate, while NCEP CFSv2 and ERA5 Q_{sfc} are 0.21 PW (or 31%) and 0.18 PW (or 27%) weaker, respectively. According to the error bars, the differences for NCEP CFSv2 and ERA5 are statistically distinct at the 1σ level (67%) over this longer period. None of the differences are statistically significant at the 2σ level (95%).

3.4. Subpolar salinity and freshwater exchange derived from OSNAP

There is a net poleward salinity transport across the OSNAP array, which is 12.5 ± 1.0 Sv for 2014–2018. The uncertainty in the time-mean salinity transport includes the standard error of the 4-year mean transport (0.3 Sv) and a possible bias error (0.7 Sv; derived from the same datasets in Li et al., 2017). This net salinity transport is related to the dilution of the poleward-flowing salty Atlantic waters ($S\sim35.3$) into the equatorward-flowing fresher NADW ($S\sim34.9$; Fig. S6). The former is mainly contained in the AMOC upper limb within the main branches of the NAC in the eastern Iceland basin and the Rockall Trough, while the latter is contained in the lower limb through the deep boundary currents across the Labrador, Irminger and Iceland basins (Fig. 6). In total, the net salinity transport is a residual between the poleward salinity transport of 540.7 Sv in the AMOC upper limb (corresponding to a mean volume transport of 16.6 Sv, Li et al., 2021), and the equatorward salinity export of 528.2 Sv in the lower limb.

Salty waters in the NAC branches east of the central Iceland basin (753.2 Sv) constitute the main poleward salinity transport across the OSNAP line, which is largely compensated by a net equatorward salinity transport through the Labrador, Irminger and western Iceland basins (-740.7 Sv). We have also estimated the transport associated with the main boundary currents intercepted by the OSNAP boundary arrays. There is a salinity transport in the main NAC branch of 563.5 Sv in the eastern Iceland basin and 235.8 Sv in the Rockall Trough (see Table S3 for the corresponding volume transport and salinity). Some of the transport recirculates in the western Iceland basin flowing equatorward via the ERRC of -530.8 Sv and then poleward again via the IC of 230.7 Sv. The stronger currents at both sides of Greenland contribute to larger salinity transports, with -1094.8 Sv in the EGC and 1158.4 Sv in the WGC. Finally, the LC exits the Labrador Sea with a salinity transport of -1155.5 Sv.

There is a net equatorward (poleward) salinity transport of 49.5 \pm 1.6 Sv (62.0 \pm 1.2 Sv) across OSNAP West (East). The uncertainties contain both the standard error in the 4-year mean salinity transport (1.1 and 1.0 Sv for OSNAP West and East, respectively), and a possible bias error (0.5 and 0.2 Sv for OSNAP West and East, respectively). Most of the salinity transports across OSNAP West and East are accounted for by the non-zero throughflow at the respective section (Table S5). The

Table 3

Surface freshwater exchange for the broader-Arctic region associated with the oceanic transports across major gateways. All values are the time-mean plus/minus uncertainty. The uncertainty in the freshwater exchange derived from OSNAP includes the standard error in the 4-year mean estimate (0.01 Sv for all sections), a possible bias error (0.03, 0.01, and 0.01 Sv for the full OSNAP array, OSNAP West and East, respectively, Li et al., 2017), and an error related to sea ice transports (~0.01 Sv). The uncertainty in FW_{sfc} is derived by combining the component errors in quadrature. Positive (negative) values indicate freshwater sources (sinks) for the respective ocean basin.

| | OSNAP | Bering Strait | FW_{sfc} | OSNAP West | Davis Strait | FW_{sfc} | OSNAP East | Fram Strait | Barents Sea Opening | FW_{sfc} |
|--------------------|--|-----------------------|-------------|---|---------------------------------|---|---|------------------------|------------------------|----------------|
| Freshwater (Sv) | $\begin{array}{c} \textbf{0.36} \; \pm \\ \textbf{0.05} \end{array}$ | -0.08 ± 0.004^{a} | 0.28 ± 0.05 | $\begin{array}{c} 0.18 \pm \\ 0.04 \end{array}$ | $-0.105 \pm 0.006^{\mathrm{b}}$ | $\begin{array}{c} \textbf{0.08} \pm \\ \textbf{0.04} \end{array}$ | $\begin{array}{c} 0.18 \pm \\ 0.03 \end{array}$ | -0.147 ± 0.016^{c} | 0.004 ^d | 0.04 ± 0.03 |

a Liquid OFT estimate based on the measurements of non-Alaskan Coastal Current (ACC) transport of 66 ± 4 mSv (poleward) with a correction for the unresolved portion of the ACC (6 ± 2 mSv) and restratification (4 ± 1 mSv), with a reference salinity of 34.8 (2003–2015, Woodgate, 2018). Adjusted to the Bering Strait-OSNAP boundary-mean salinity of 34.93, it gives the Bering Strait's contribution to the FW_{sfc} for the ocean between the Bering Strait and the full OSNAP line of -80 ± 4 mSv. b Liquid OFT is 93 ± 6 mSv (equatorward; at salinity ~ 33.78) and OFT via sea ice is 10 ± 1 mSv (equatorward; at salinity of 5), with a reference salinity of 34.8 (2004–2010, Curry et al., 2014). Adjusted to the Davis Strait-OSNAP West boundary-mean salinity of 34.85, it gives the Davis Strait's contribution to the FW_{sfc} for the ocean between the Davis Strait and the OSNAP West line of -105 ± 6 mSv.

Table 4

Extratropical North Atlantic freshwater budget (units: Sv). The observation-based FW_{sfc} estimate is obtained as the sum of FW_{adv} and FW_{oSC} . FW_{sfc} from atmospheric reanalysis products are also shown for comparisons. The uncertainty in the time-mean estimate from RAPID contains the standard error in the time-mean of 0.02 for 2014–2018 and 0.01 Sv for 2004–2018, respectively, along with a potential bias error of 0.01 Sv (McDonagh et al., 2015). FW_{oSC} is the ensemble mean derived from four gridded salinity datasets (Appendix B). The uncertainty in FW_{adv} and in the observation-based FW_{sfc} are derived by combining the component errors in quadrature. Positive (negative) values indicate freshwater sources (sinks) for the respective ocean basin.

| | OSNAP F | RAPID | Strait of Gibraltar | FW_{adv} | FWosc | FW_{sfc} | | | |
|---------------|-----------------|-----------------|---------------------|-----------------|----------------|----------------|----------------------|----------------------|-----------------|
| | | | | | | Observation | NCEP CFSv2 | JRA55 | ERA5 |
| 8/2014-5/2018 | -0.36 ± 0.0 | 0.42 ± 0.03 | 0.03 ± 0.01 | 0.09 ± 0.06 | -0.15 ± 0.09 | -0.06 ± 0.11 | -0.11 ± 0.01 | -0.19 ± 0.01 | -0.14 ± 0.01 |
| 4/2004-8/2018 | -0.36 ± 0.0 | 0.43 ± 0.02 | | 0.10 ± 0.07 | -0.05 ± 0.02 | 0.05 ± 0.07 | -0.11 ± 0.01^{b} | $-0.19\; {\pm}0.005$ | -0.15 ± 0.004 |
| | а | | | | | | | | |

^a Data available for August 2014–May 2018. Note that we add 0.02 Sv to the uncertainty estimate to account for possible errors over longer periods.

throughflow corresponds to an equatorward (poleward) salinity transport of 55.6 Sv (55.9 Sv) at OSNAP West and East, respectively. The residual salinity transport (related to the overturning and isopycnal circulations) is nearly the same for both sections: a poleward transport of 6.0 Sv across OSNAP West and 6.1 Sv across East, in which the overturning component accounts for the larger portion (\sim 60%).

The surplus salinity across OSNAP to higher latitudes corresponds to a positive surface freshwater input of 0.36 Sv for the basin between the Bering Strait and OSNAP (Table 3). Similar to the heat transport, we stress that the omission of the Bering Strait throughflow across the entire OSNAP section has a negligible impact on the freshwater exchange (i.e., one magnitude smaller than the uncertainty, see Appendix A). This is a component of the surface freshwater exchange (FWsfc) for the region, which is induced by the oceanic volume and salinity transports across the OSNAP line. The freshwater is added to dilute the salty inflowing waters, producing the relatively fresh deep waters flowing equatorward across the OSNAP line. Since there is no net mass flux across the entire OSNAP section, the corresponding FW_{sfc} for the region equals the salinity transport across OSNAP scaled by $1/\overline{S}$ ($\overline{S} = 34.93$ is the mean salinity of the bounding sections of the domain, Appendix A). This linear relationship between the salinity transport and FWsfc also applies to the overturning and isopycnal components because there is also no net mass flux associated with these circulations (Fig. 7a). For our subsequent analysis, we will focus only on freshwater inputs at the surface (FW_{sfc}) rather than on salinity transports at OSNAP and elsewhere.

The surface freshwater input derived from the full OSNAP array

shows monthly variations that range from 0.26 to 0.47 Sv (Fig. 7a). There appears to be a seasonal variation in the second half of the record (2016-2018), with maximum (i.e., largest freshwater input) in winter, but no such cycle is apparent during the first two years. The overturning and isopycnal components appear to have seasonal variations that tend to cancel each other. The overturning component accounts for the larger portion (60%) of the total, with thus a significant contribution from the isopycnal component (Table S6). The isopycnal component actually exceeds the overturning component each fall. The results are consistent with the early published shorter record (Lozier et al., 2019). The seasonal variations in the overturning and isopycnal components are related to the seasonal cycle in the volume transports in the region. which is similar to the heat transports in the region as mentioned earlier. In addition, the seasonality in the overturning component is modulated by the seasonal cycle in the Labrador Current above the Labrador shelf, which is strongest during January-March each year (see also Fig. 7b).

Neither overturning nor isopycnal component dominates the variability in the OSNAP salinity transport and the corresponding freshwater input, with the overturning and isopycnal components explaining only 40% and 23% of the total variance, respectively. The reduced (increased) contribution from the overturning (isopycnal) component is associated with fresher water masses originated in the Arctic-subarctic region passing through the subpolar latitudes while not participating in the overturning (Østerhus et al., 2019; Le Bras et al., 2020). Those are the freshest waters at the OSNAP array, flowing equatorward mainly via the coastal currents above the Labrador Shelf (Han et al., 2019) and the

^c Liquid OFT is 89 ± 13 mSv (equatorward; at salinity ~ 33.25) and OFT via sea ice is 60 ± 9 mSv (equatorward; at salinity of 4), with a reference salinity of 34.8 (2000–2010, Haine et al., 2015). Adjusted to the Fram Strait-Barents Sea Opening-OSNAP East boundary-mean salinity of 34.77, it gives the Fram Strait's contribution to the FW_{sfc} for the ocean bounded by Frame Strait-Barents Sea Opening and OSNAP East of -147 ± 16 mSv.

d OFT estimate based on a volume transport of 2 Sv for Atlantic Waters into the Barents Sea at salinity ~ 35.1 , 1.2 Sv for the Norwegian Costal Current into the Barents Sea at salinity ~ 34.34 , and 1.2 Sv out of the Barents Sea through the Bear Island Trench at salinity ~ 35 (1997–2007, Smedsrud et al., 2010). Adjusted to the Fram Strait-Barents Sea Opening-OSNAP East boundary-mean salinity of 34.77, it gives the Barents Sea Opening's contribution to the FW_{sfc} for the ocean bounded by Fram Strait-Barents Sea Opening and OSNAP East of 4 mSv.

^b Data available for January 2011–August 2018.

East Greenland Shelf (de Steur et al., 2018; Foukal et al., 2020; Le Bras et al., 2018).

OSNAP West and East have comparable contributions to the surface freshwater input over the Bering Strait-OSNAP region. Their time-means are the same of 0.18 Sv, with a slightly larger uncertainty at OSNAP West (0.03 Sv) than East (0.02 Sv). In terms of the variability, OSNAP East explains the slightly larger portion (56%) of the variance in the total freshwater input induced by the OSNAP transports (comparing the solid black lines in Fig. 7a and 7b). Overall, it highlights the importance of the Labrador Sea in the freshwater budget in the subpolar basins, which is in contrast to the Labrador basin's marginal contribution to the heat budget.

At OSNAP West, the overturning component dominates the surface freshwater input (Fig. 7b and Table S6), which accounts for 67% of the mean and explains 84% of the variance. There, the corresponding freshwater input exhibits seasonal cycles that are mostly contained in the overturning component, which has maximum (i.e., largest freshwater input) in each winter. It is associated with the seasonality of the overturning circulation in the basin (Holte; Straneo 2017; Li et al., 2021), and is enhanced by the seasonality in the currents above the Labrador shelf that carry the freshest and thus lightest water mass from the Arctic Ocean (Han et al., 2008; Wang et al., 2015). A smaller part of the seasonal signal is contained in the isopycnal component (33% of the mean), which has minimum in fall. It is associated with the transport variation of the salty Irminger Water in the WGC (Pacini et al., 2020). At OSNAP East, there are significant contributions from both the overturning and isopycnal components (Fig. 7c). However, the contribution from the overturning component is slightly smaller than OSNAP West, which accounts for 61% of the mean and explains 61% of the variance. As mentioned above, this complex pattern follows mixed sources of salinity transports across the eastern subpolar gyre. The overturning component shows weak seasonality, associated with the seasonal variations in the MOC across OSNAP East (Li et al., 2021).

We do not measure any sea ice transports across OSNAP when estimating the salinity transport. The contributions via sea ice have been suggested to be small, e.g., in the annual-mean OFT of the LC (Han et al., 2019; Mertz et al., 1993) and the EGC (Bacon et al., 2014). Based on those earlier studies, we estimate that the sea ice contributes to <3% (or ~ 0.01 Sv) of the FW $_{sfc}$ estimated from OSNAP, which is included as part of the uncertainty estimate in the derived freshwater exchanges (see Table 3).

3.5. Surface freshwater exchange between OSNAP and Bering Strait

The OSNAP observations are combined with historical estimates at main straits of the Arctic Ocean to derive the surface freshwater exchange for individual subdomains with the wider Arctic region, assuming no net freshwater storage over the region. Note that the transport estimate at different locations represents the mean condition over the respective time period (Table 3). The results indicate a net freshwater input of 0.28 Sv for the region between OSNAP and the Bering Strait (see also Fig. 8). Additionally, we estimate a freshwater input of 0.08 Sv for the Labrador Sea between the Davis Strait and OSNAP West, and 0.04 Sv for the subarctic-subpolar region between the Fram Strait-Barents Sea Opening and OSNAP East.

We cannot say with certainty that the observation-based estimates are representative of long-term averages for the region, due to the fact that the volume and salinity transport estimates across the main Arctic straits are based on observations from the 2000 s, while the OSNAP record is only available for 2014–2018. Further, unlike the heat transport divergences that are dominated by the OSNAP heat transports, the surface freshwater exchange for the subdomains is strongly affected by the relatively fresh waters exported from the Arctic Ocean. As such, the OSNAP's contribution to the surface freshwater input for the subarctic-subpolar regions is comparable to the contribution from the Arctic inflows across the Davis and Fram Straits (Table 3). However, previous

studies suggest a weak decadal transport at the Bering Strait (<0.01 Sv, Haine et al., 2015; Wang et al., 2016), therefore the estimate of the OSNAP-Bering Strait transport divergence may represent well the 2014–2018 condition. By comparison, our uncertainty estimates likely stand for lower bounds for the two subarctic-subpolar domains, which could be ~ 0.01 –0.02 Sv larger when considering the decadal variations in the freshwater transports across the Arctic straits (Wang et al., 2016). Longer OSNAP records will be needed to evaluate how representative these observational estimates of climatological averages.

3.6. Surface freshwater exchange between OSNAP and RAPID

3.6.1. Salinity transport and surface freshwater exchange derived from RAPID

The 2004–2018 mean salinity transport is 15.1 \pm 1.0 Sv across RAPID. The uncertainty includes the standard error in the 14-year mean of 0.8 Sv, and a potential bias error of 0.2 Sv (McDonagh et al., 2015). The observed salinity transport corresponds to a freshwater input of 0.43 \pm 0.02 Sv over the ocean basin between the Bering Strait and the RAPID line.

It is worth understanding the terminology and methodology differences between the FW_{sfc} derived from the RAPID array presented here, and an earlier estimate of the net transport across the RAPID array referred to as the freshwater flux or the OFT (that is 1.17 Sv equatorward for 2004-2012, McDonagh et al., 2015). In McDonagh et al., the OFT includes (i) 0.8 Sv of seawater flowing through the Bering Strait and subsequently the RAPID line, and (ii) 0.37 Sv of freshwater added through the surface of the ocean between the Bering Strait and the RAPID line (denoted as the 'freshwater divergence'). They further decomposed the freshwater divergence into the throughflow component of -0.06 Sv, and 0.43 Sv carried by the overturning (-0.78 Sv) and horizontal circulation (0.35 Sv). Our estimate of the 0.43 Sv FW_{sfc} can be thought of as one component of the OFT reported by McDonagh et al., and is the correspondent of the 'equivalent freshwater flux' (totaling -0.43 Sv) across the RAPID array given in (Table 1 in McDonagh et al. (2015)

The subtropical oceanic transports cause a larger and more variable freshwater exchange than the subpolar transports. For the OSNAP time period between 2014 and 2018, the RAPID salinity transport is 14.7 \pm 0.7 Sv and the corresponding freshwater input is 0.42 \pm 0.03 Sv. This surface freshwater input is $\sim 17\%$ stronger than that derived from OSNAP, and its standard deviation (0.18 Sv) is \sim 3 times larger than OSNAP (0.05 Sv; Fig. 9). Further partition between the mass-balanced portion of the circulation reveals that the overturning circulation causes a freshwater input from the atmosphere to the ocean, with a stronger overturning component of the freshwater input north of the RAPID line (0.78 Sv, McDonagh et al., 2015) compared to that north of OSNAP (0.21 Sv). In addition, the gyre (horizontal) component in the subtropics $\,$ creates a loss of freshwater north of RAPID (-0.35 Sv, McDonagh et al., 2015), partially cancelling out the overturning component. On the contrary, the gyre (isopycnal) component in the subpolar region causes a freshwater gain north of OSNAP (0.14 Sv), thus complementing the overturning's contribution in the region.

There is a strong linear relationship between the OFT and the strength of the overturning circulation at RAPID, which describes about 90% of the variance (McDonagh et al., 2015). It thus indicates a dominating role of the overturning circulation in the subtropical salinity transport and its effect on the surface freshwater exchange north of the RAPID line. This contrasts with the subpolar freshwater exchanges: there is not a robust linear relationship between the subpolar overturning and the salinity transport across OSNAP (and thus the corresponding surface freshwater input). As discussed earlier, the overturning circulation at OSNAP only explains 40% of the total variance in the surface freshwater input.

The larger freshwater input north of RAPID than that north of OSNAP reflects a net freshwater input over the extratropical region between the

two sections. The time-mean of this freshwater input is 0.06 Sv during 2014-2018, and its temporal variability is dominated by the RAPID transports (Fig. 9). Such an input corresponds to an addition of freshwater from the atmosphere into the ocean to balance (dilute) the surplus salinity convergence in the region. Additionally, the salinity transport through the Strait of Gibraltar should be taken into account when estimating the surface freshwater exchange over the region. Though the net volume transport through SG is negligible (~0.035 Sv, Criado-Aldeanueva et al., 2012), the salty Mediterranean Outflow Water considerably affects the salt content in the North Atlantic, and thus contributes to the surface freshwater exchange (Appendix A). Collectively, we estimate that there is an addition of freshwater for the extratropical North Atlantic of 0.09 Sv during the 2014-2018 time period. That is, a net freshwater gain is needed to balance the salinity transports across the entire OSNAP-Strait of Gibraltar-RAPID boundary (denoted as FWady, Table 4).

A change in the OSC also corresponds to a surface freshwater exchange. During 2014–2018, basin-wide salinity indicates that the ocean between OSNAP and RAPID experienced a freshening from early 2015 to mid 2016 that reversed the preceding salinification in late 2014, which was followed by a year-long salinification through 2017 (Fig. S7). This pattern of the basin-wide OSC variability reflects an addition of freshwater between early 2015 and mid 2016, with net removal of freshwater before and after (Fig. S5a). There is an overall salinity increase during 2014–2018, which gives rise to a time-mean FW_{OSC} of -0.15 Sv. Taking into account all the salinity changes, we estimate a FW_{sfc} of -0.06 Sv during 2014–2018, which represents a freshwater removal from the region between OSNAP and RAPID (Table 4 and Fig. 8). There is no clear indication of a seasonal variation in either FW_{OSC} and FW_{sfc} ; therefore, we use the full length of the record for the mean estimates without considering any seasonal biases.

3.6.2. Comparison with atmospheric reanalyses

The net surface freshwater flux (evaporation minus precipitation plus water run-off) from NCEP CFSv2, ERA5, and JRA55 have been integrated over the surface area between OSNAP and RAPID (1.9 \times $10^{13}m^2$) to derive the FW_{sfc} in Sv. All three products show consistently negative FW_{sfc} (a net loss of freshwater from the ocean to the atmosphere) for the 2014-2018 period and have comparable temporal variability on monthly-to-interannual time scales (Fig. S5). The FW_{sfc} are comparable in NCEP CFSv2 (-0.11 Sv) and ERA5 (-0.14 Sv), which are \sim 40% weaker than JRA55 (-0.19 Sv) (Table 4). The associated uncertainty in the products is the same (0.01 Sv), which only includes the standard error in the time-mean estimates. Comparing these time-mean estimates to the observations reveal a difference of up to 0.13 Sv in JRA55, which is statistically significant at the 1σ level (67%). By comparison, the difference is 0.05 Sv in NCEP CFSv2 and 0.08 Sv in ERA5, which are not statistically distinct at the 1σ level (67%). None of the observation-reanalysis differences are statistically significant at the 2σ level (95%)

We next consider the surface freshwater exchange for the whole length of the RAPID record from April 2004 to August 2018. Similar to the subpolar heat transport, decadal variations in the subpolar freshwater transports are weak (\sim 0.01–0.02 Sv, Li et al., 2017; Rossby et al., 2017), which can be thought of as an additional error in the transport estimate over the 2004–2018 period (see Table 4). The longer records yield a FW_{sfc} of 0.04 Sv during 2004–2018, indicating a net freshwater input from the atmosphere to the ocean. The change in the mean estimate from -0.06 Sv to 0.04 Sv is mainly due to the change in the salinity storage (the FW_{OSC} term). It reflects a long-term salinification during 2004–2018, but at a much weaker rate than occurred during 2014–2018, by approximately a factor of three (Table 4; Fig. B.2). In the meantime, changes in the oceanic transports caused a marginal difference in the freshwater divergence (FW_{adv}), which is 0.01 Sv (or \sim 10%) stronger during 2004–2018 than 2014–2018 and is however not

statistically significant according to the error bars.

For the extended time period, only the ERA5 estimate shows a small change of 0.01 Sv (Table 4). All reanalysis products show consistently a net freshwater loss from the ocean to the atmosphere, in contrast to the observational estimates showing an addition of freshwater from the atmosphere to the ocean. The comparisons show an observation-reanalysis difference of 0.16–0.24 Sv, which are all statistically significant at the 1σ level (67%). At the 2σ level (95%), only JRA55 and ERA5 show distinct differences with observations.

4. Discussion

The OSNAP array has resulted in 4-year continuous measurements of the trans-basin volume, heat and salinity transports in the subpolar region. We use these transports to derive surface heat and freshwater exchanges across the surface area of the adjacent ocean basin, based on the budget analyses. A majority of the subpolar heat transport is contained in the eastern subpolar gyre, which has profound implications for the strength of deep convection (e.g., by affecting the stability of the water column) north of the OSNAP East line that has been linked to the subpolar overturning variability (Lozier et al., 2019). Although the Labrador Sea's deep convection is suggested to play a minimal role in the strength of the subpolar overturning in density space (Lozier et al., 2019), the basin accounts for half of the surface freshwater input created by the OSNAP transports. The subsequent export of the freshwater input in the Labrador Sea as well as its downstream pathways can exert a considerable influence on salinity anomalies within the subpolar gyre (Holliday et al., 2020).

In contrast to the dominant role of the overturning circulation in the subtropical heat and salinity transports (and the corresponding surface freshwater exchange), variability in the subpolar transport/exchange arise from both the overturning and isopycnal component of the circulation. The overturning component plays a less dominant role in the subpolar gyre's salinity and freshwater changes, a considerable portion of which originates from higher latitudes that does not participate in overturning (Le Bras et al., 2020). Furthermore, our results suggest a plausible linkage between changes in the intensity of the subpolar gyre circulation and changes in the water properties at the subpolar latitudes. The latter is expected to affect the strength of the deep convection, which implies an underlying gyre-convection connectivity that may explain profound property changes in the subpolar region over longer time scales (Fu et al., 2020) and is suggested to have delayed impact on the overturning circulation (Menary et al., 2015; Ortega et al., 2015). Finally, the decreased (increased) contribution from the overturning (isopycnal) circulation to the freshwater input in the subpolar North Atlantic also raises a question as to whether the overturning component of the OFT itself can be used as a robust indicator of the freshwater feedback during a changing AMOC (Mignac et al., 2019).

A combined analysis of the OSNAP transports with estimates from trans-basin arrays at other locations provides key constraints for the strength of oceanic heat and salinity transports as well as the resultant surface freshwater exchange over the broad Arctic-North Atlantic region. Our results indicate that the heat transport convergence in the extratropical North Atlantic basin south of the OSNAP line (0.68 PW) is $\sim 30\%$ larger than that in the broader-Arctic domain north of OSNAP (0.51 PW). In contrast, the surface freshwater input over the extratropical North Atlantic (0.09 Sv) is only $\sim 30\%$ of that over the broader-Arctic region (0.28 Sv). In addition, our results reveal distinct patterns of the surface heat and freshwater exchanges in the subarctic-subpolar regions. The subarctic-subpolar region east of Greenland dominates the surface heat exchange, while the Labrador Sea contributes more to the freshwater exchange,

Our above estimates of the surface heat and freshwater exchange north of the OSNAP latitudes are in good agreement with previous observation-based estimates for the broader-Arctic region. Specifically, the surface heat loss of 0.51 PW between OSNAP and Bering Strait is similar to an earlier estimate of 0.47 PW heat loss over the same region, which includes 0.31 PW over the Arctic Mediterranean (Tsubouchi et al., 2021), 0.04 PW for the Labrador Sea and 0.122 PW over the region between 60°N and the Greenland-Scotland Ridge (Chafik; Rossby, 2019). As for the freshwater exchange, our estimate of a freshwater input of 0.28 Sv over between OSNAP and Bering Strait is slightly weaker than an estimate of 0.34 Sv freshwater input obtained by combining 0.20 Sv for the Arctic and the Barents Sea (Tsubouchi et al., 2018), 0.04 Sv for the Nordic Seas (Segtnan et al., 2011), and 0.10 Sv for the region between 60°N and the Greenland-Scotland Ridge as well as the Labrador Sea (Chafik; Rossby, 2019).

Finally, we estimate the net surface heat (freshwater) exchanges by taking into account the observed OHC (OSC) changes. Comparing the observation-based estimates with the air-sea flux from the atmospheric reanalysis products shows an overall consistent pattern over the North Atlantic basin during the observation periods. During the 2014-2018 overlapping time period of all records, we find statistically significant bias errors in the surface heat and freshwater fluxes from JRA55 (both at the 67% level). The results are in line with previous studies showing anomalously large latent and sensible heat fluxes from JRA55 compared to the NCEP and ERA products (Cronin et al., 2019; Yu, 2019). The observation-reanalysis differences in the surface heat flux (~5-10 W m⁻²) are smaller than the biases in reanalyses reported in earlier works in the region (e.g., \sim 10–30 W m⁻², Josey, 2001). The differences in the surface freshwater exchange (~0.1 Sv or 17 cm yr⁻¹) is in line with the known uncertainty in the surface freshwater flux products as indicated by the large spread among different reanalyses across mid- to highlatitude regions? of the North Atlantic (~20 cm yr⁻¹, Yu, 2019). Over the longer 2004-2018 time period, comparisons between observation and the reanalysis products show similar differences in the surface heat transport but larger discrepancies in the surface freshwater exchange (up to ~ 0.2 Sv or 33 cm yr⁻¹) over the North Atlantic domain.

Our work presents a framework for evaluating potential errors in the surface heat and freshwater fluxes derived from atmospheric reanalyses. The magnitude of these errors has been thought to cause large discrepancies in estimates of the surface-forced overturning circulation (Grist et al., 2014) and in the inferred meridional ocean heat transports (Valdivieso et al., 2017). Longer trans-basin observations in both the subpolar and subtropical latitudes will undoubtedly improve the assessment of the potential biases in air-sea fluxes that we offer here.

Declaration of Competing Interest

The authors declare that they have no known competing financial interests or personal relationships that could have appeared to influence the work reported in this paper.

Acknowledgements

We thank Elaine McDonagh for insightful comments and discussions on the heat and freshwater analysis. F.L. and M.S.L. were supported by the National Science Foundation (OCE-1948335). W.E.J. was supported by the National Science Foundation grants RAPID (OCE-1332978 and OCE-1926008) and OSNAP (OCE-1756231 and OCE-1948198). I.A.L.B. was supported by the National Science Foundation (OCE-1756272 and OCE-2038481). B.M. was supported by the UK Natural Environment Research Council for the RAPID-AMOC program and the ACSIS program (NE/N018044/1). S.A.C. and N.P.H. were supported by UK NERC National Capability programmes the Extended Ellett Line and CLASS (NE/ R015953/1), NERC grants UK OSNAP (NE/K010875/1, NE/K010875/2, NE/K010700/1), UK OSNAP Decade (NE/T00858X/1, NE/T008938/1), S.A.C. received additional supports from the Blue-Action project (European Union's Horizon 2020 research and innovation program, grant 727852) and the iAtlantic project (European Union's Horizon 2020 research and innovation program, grant 210522255). The RAPID dataset and associated heat and freshwater transports are made freely available online (http://rapid.ac.uk/rapidmoc). OSNAP data were collected and made freely available by the OSNAP (Overturning in the Subpolar North Atlantic Program) project and all the national programs that contribute to it (www.o-snap.org). EN4 monthly mean subsurface temperature and salinity profiles are made freely available by the Met Office (http://www.metoffice.gov.uk/hadobs/en4).

Appendix A. Surface freshwater exchange

Derivation of sea surface freshwater exchange from oceanic variables

Based on water mass and salt conservation, the salt mass transport across the boundary of an enclosed ocean basin together with the salt content change within the basin can be related to different components of the true freshwater exchange across the surface of that basin. The reader is referred to Bacon et al. (2015) for the full derivation, and here we only cover the key aspects.

Salt mass is conserved within the enclosed volume, *V*, and there is no salt mass flux across the sea surface. Therefore, the salt mass flux across the boundary of the basin must equal the time rate of change of salt mass within it:

$$\iint S\rho v dx dz = \iiint \frac{\partial (S\rho)}{\partial t} dV, \tag{A1}$$

where S is sea water salinity.

The salt mass flux across the boundary can be decomposed into components related to distinct elements of water mass flux, ρv , across the boundary: the net flux and the remaining mass-balanced flux, i.e., $\rho v = \overline{\rho v} + (\rho v)$. Overbar indicates boundary mean and prime indicates anomalies from the mean. Integrating $\overline{\rho v}$ along the whole boundary gives the net mass flux across the boundary, which always results in a salt mass flux given the fact that $S \neq 0$ in the ocean. Integrating (ρv) along the whole boundary yields a zero-mass flux, which can result in a salt mass flux when salinity is distributed non-uniformly across the boundary. Accordingly, the salt mass flux across the boundary are related to the two components of S, i.e., $S = \overline{S} + S'$, where \overline{S} is the boundary-mean salinity, and S' are deviations from the mean. The boundary salt mass flux in Eq. (A1) can be broken down as:

$$\iint S\rho v dx dz = \iint \left(\overline{S} + S'\right) \left[\overline{\rho v} + (\rho v)'\right] dx dz = \overline{S} \iint \overline{\rho v} dx dz + \iint S'(\rho v)' dx dz$$
(A2)

The first term on the right-hand side (RHS) of Eq. (A2) is the salt mass flux associated with the net mass flux across the boundary multiplied by \overline{S} . It only depends on the boundary-mean salinity. This is because that the contributions from positive or negative salinity anomalies (S') associated with the net mass flux cancel out each other and altogether yields no salt mass flux. The second term on the RHS of Eq. (A2) is the salt mass flux associated with the compensated inflow and outflow that are at different salinities.

The net mass flux across the boundary, $\overline{\rho v}$, can be estimated as the difference between the time rate of change of total water mass within the basin,

M, and the mass flux across the surface area of the basin (F_{sfc}^m). Then by rearrange Eq. (A2) and using Boussinesq approximation, surface freshwater volume flux can be expressed as:

$$FW_{sfc} = \frac{1}{\overline{S}} \iint S'v' dxdz + \frac{dV}{dt} - \frac{1}{\overline{S}} \left[\frac{\partial}{\partial t} \iiint SdV \right]$$
(A3)

 FW_{sfc} is the freshwater volume exchange across the surface of the ocean, whose meaning is clear and unambiguous. The RHS of Eq. (A3) includes the different FW_{sfc} components: The first term is the FW input created by the salt flux across the whole boundary, referred to as FW_{adv} , which resembles the traditional definition of oceanic freshwater transport. FW_{adv} is associated with the salinity change between the inflowing and outflowing waters at the boundary. For example, if waters flowing into the basin are more saline than waters flowing out, it requires a positive FW_{adv} (that is an addition of freshwater) to account for this change. FW_{adv} can be estimated based on direct velocity and salinity observations. The second term of the RHS of Eq. (A3) is the time rate of change of the total water volume, FW_{vol} . This term is associated with the mass-induced sea level variations, which can be estimated by subtracting the steric component from the total sea level changes. This term is typically negligible as will be shown next. The third term of the RHS of Eq. (A3) reflects a storage change of salinity in the basin, which we referred to as FW_{OSC} . Its relationship with FW_{sfc} is straightforward: a freshening basin (decreasing S) corresponds to a positive FW_{sfc} . This term can be estimated from salinity measurements within the ocean basin.

Eq. (A3) allows for an 'indirect' way for deriving a meaningful surface freshwater transport based on accurate measurements of sea water velocity, salinity and temperature.

Water volume change (FW_{vol})

The time rate of change in the total water volume can be estimated using the mass-induced sea level variations, i.e.,

$$FW_{vol} = A \frac{\partial (\dot{\eta'} - \dot{\eta'_{st}})}{\partial t},\tag{A4}$$

where A is the total surface area of the study domain, η is the total sea level anomaly obtained from satellite observations, and η_{st} is the steric component derived from hydrographic data (i.e., in relation to changes in the density of the water column). Using the satellite altimetry (produced and distributed by the Copernicus Marine and Environment Monitoring Service; http://marine.copernicus.eu) and EN4 datasets, we estimate this change in the North Atlantic basin between OSNAP and RAPID to be -0.004 Sv (-0.0004 Sv) during the 2014–2018 (2004–2018) time period. That is, the total sea level changes mostly represent the steric sea level changes, with the contribution from the mass changes being negligible over seasonal and longer time scales.

Surface freshwater exchange derived from the OSNAP observations

Even though the derivation of FW_{sfc} requires salinity transport information from the whole boundary, we can determine its fraction associated with the salinity transport across any part of the boundary once we have defined the boundary means as mentioned above. We take OSNAP as an example, and show how a surface freshwater exchange is inferred from the velocity and salinity measurements from the array, e.g., by considering the impact of the salinity transport across OSNAP on the salt content north of the line all the way north to the Bering Strait. At OSNAP, the section-mean salinity is 34.93 during August 2014–May 2018, with a total area of $0.70 \times 10^{10} m^2$. The cross-sectional area at the Bering Strait is approximately $4.2 \times 10^6 m^2$ with a section-mean salinity of 32.47. Given the huge area difference between these two sections, the Bering Strait-OSNAP boundary-mean salinity (\bar{S}) and mean velocity (\bar{v}) are the same as the OSNAP section means. Then, the surface freshwater exchange associated with the OSNAP transports can be expressed as

$$FW_{sfc} = \frac{1}{\overline{S}} \iint (S_o - \overline{S})(v_o - \overline{v}) dx_o dz_o, \tag{A5}$$

where S_0 , v_0 are salinity and inwards-positive velocity measured by the OSNAP array, x_0 and z_0 are horizontal and vertical coordinates at OSNAP. Because the volume flux is conserved at OSNAP ($\sqrt[n]{v_0}dx_0dz_0 = 0$; (Lozier et al., 2019)), Eq. (A5) is reduced to,

$$FW_{sfc} = \frac{1}{5} \iint S_o v_o dx_o dz_o. \tag{A6}$$

That is, the surface freshwater exchange is the OSNAP salinity transport scaled by $1/\overline{S}$. Monthly standard deviation in \overline{S} is up to 0.003 over the observational period, which leads to typical errors of \sim 0.01% in FW_{sfc} and is negligible.

Error in surface freshwater exchange related to a neglected throughflow

A throughflow traversing an enclosed ocean basin can result in a salt content change, e.g., due to the change in salinity at which the throughflow enters and leaves the basin. However, a trans-basin array that relies on dynamic height moorings typically applies a zero-net-throughflow constraint when calculating the cross-sectional velocities (Lozier et al., 2019; McCarthy et al., 2015). Therefore, it neglects the throughflow across the array as shown in Eq. (A5), and inevitably introduces an error in the FW_{sfc} estimate.

Taking OSNAP as an example, there is a throughflow at the Bering Strait of 1 Sv into the Arctic Ocean (Woodgate, 2018) that subsequently flows equatorward across the OSNAP section. This throughflow has been neglected at OSNAP as mentioned earlier. If we allow for a throughflow at OSNAP, then $\iint v_o dx_o dz_o \neq 0$. The errors associated with the throughflow can be estimated as part of Eq. (A5) concerning the salinity transport due to the net throughflow velocity \bar{v} :

$$FW_{throughflow} = \frac{1}{\overline{S}} \iint (S_o - \overline{S}) \overline{v} dx_o dz_o. \tag{A7a}$$

As \overline{v} and \overline{S} are constant, we denote $\overline{S_o}$ as the section-mean salinity at OSNAP ($\overline{S_o} = \iint S_o dx_o dz_o / \iint dx_o dz_o$), and then we can write

$$FW_{throughflow} = \frac{1}{\overline{S}} \times (\overline{S_o} - \overline{S}) \times T_{throughflow}, \tag{A7b}$$

where $T_{throughflow}$ is the volume transport of the Bering Strait throughflow. Here, $FW_{throughflow}$ is zero, because in Eq. (A7b) the section-mean salinity at OSNAP $\overline{S_o}$ approximately equals the Bering Strait-OSNAP boundary-mean salinity \overline{S} .

We next compute the error for the freshwater exchange estimated in the basin bounded by the Fram Strait-Barents Sea Opening and OSNAP East. At OSNAP East, there is a net poleward volume transport of 1.6 Sv applied for conserving the mass flux across the whole OSNAP array (Lozier et al., 2019). This is probably larger than the actual poleward volume transport of 0.6 Sv that is obtained as the residual of the throughflows at the Bering (1 Sv) and Davis Straits (1.6 Sv equatorward; Curry et al., 2014). Such a 1 Sv difference in the throughflow transport leads to an error in the corresponding FW_{sfc} estimate for the basin, which can be estimated following Eq. (A7b) as,

$$FW_{throughflow} = \frac{1}{34.77} \times (34.77 - 35) \times (-1Sv) = 0.007Sv, \tag{A8}$$

where 34.77 is the boundary-mean salinity across the Fram Strait-Barents Sea Opening and OSNAP East, and 35 is the section-mean salinity at OSNAP East. The associated error is $<\sim$ 30% of the uncertainty estimate in the FW_{sfc} for the ocean basin bounded by the Fram Strait-Barents Sea Opening-OSNAP East line (0.03 Sv, Table 3).

We next consider the error for the freshwater exchange estimated in the basin bounded by the OSNAP and RAPID arrays. Because both OSNAP and RAPID apply a zero–net-throughflow constraint, the error estimate in FW_{sfc} takes into account the respective error at each section that is related to the Bering Strait throughflow. It follows,

$$FW_{throughflow} = \frac{1}{35.13} \times (34.93 - 35.18) \times 1Sv = -0.007Sv. \tag{A9}$$

where 34.93 and 35.18 are the section-mean salinity at OSNAP and RAPID, respectively, and 35.13 is the OSNAP-RAPID boundary-mean salinity given a total area of $0.7 \times 10^{10} m^2$ at OSNAP and of $3.1 \times 10^{10} m^2$ at RAPID. That can be interpreted as a removal of freshwater associated with the salinity increase of the throughflow when it travels from the OSNAP section to the RAPID section. Overall, this throughflow component is one magnitude smaller than the uncertainty estimate in the FW_{sfc} over the enclosed basin between OSNAP and RAPID (0.05 Sv, Table 4), which is thus negligible.

Contribution from the volume and salinity transports through the Strait of Gibraltar

Exchanges of water between the Atlantic Ocean and the Mediterranean Sea through the Strait of Gibraltar (SG) significantly impacts the hydrography of the North Atlantic (Rogerson et al., 2012). Here, we use climatological estimates from previous studies on the property and volume transport of water masses passing the SG, and provide an estimate of the salinity transport and its contribution to FW_{sfc} over the basin enclosed by OSNAP-RAPID-SG (Table 4). Following Eq. (A5), the freshwater transport caused by the salinity transport across the SG can be calculated as,

$$FW_{SG} = \frac{1}{\overline{S}} \iint (S_{SG} - \overline{S}) v_{SG} dx_{SG} dz_{SG}. \tag{A10}$$

where subscript 'SG' denotes values for the SG, and \overline{S} is the OSNAP–RAPID–SG boundary-mean salinity. Of note is the negligible area of the SG (7.2 × 10^4m^2) compared to that of the OSNAP or RAPID sections. Therefore, including the velocity and salinity at the SG results in no appreciable changes in the estimates at the OSNAP and RAPID sections. In a simplified form, Eq. (A10) can be rewritten as,

$$FW_{SG} = \frac{1}{\overline{S}} \times [T_{MAW} \times S_{MAW} + T_{MOW} \times S_{MAW}] - (T_{MAW} + T_{MOW}) = 0.03Sv.$$
(A11)

Eq. (A11) is based on the volume transport and salinity of the outflowing Modified Atlantic Water (MAW) into the Mediterranean Sea ($T_{MAW} = -0.82 \pm 0.05$ Sv at a salinity of $S_{MAW} = 37$), and the subsurface inflowing Mediterranean Outflow Water (MOW; $T_{MOW} = 0.78 \pm 0.05$ Sv at a salinity of $S_{MOW} = 38.5$) (Criado-Aldeanueva et al., 2012; Rogerson et al., 2012; Sanchez-Roman et al., 2009; Soto-Navarro et al., 2010). The uncertainty in FW_{SG} is 0.01 Sv, estimated by considering the transport uncertainty for T_{MAW} (0.05 Sv) and T_{MOW} (0.05 Sv) (Criado-Aldeanueva et al., 2012).

Appendix B. Mean and uncertainty estimates for QOHC and FWOSC

We use four gridded temperature products (Table S1) for deriving Q_{OHC} over the North Atlantic basin between the OSNAP and RAPID lines. This is obtained from the difference of the OHC estimates for the first and last months of a given observation period, following Eq. (5). Uncertainty in the Q_{OHC} is calculated based on the uncertainty in the OHC estimate for those two months following standard error propagation theory (e.g., Thomson; Emery, 2014).

Uncertainty in the monthly OHC estimates can arise from two sources of error: (1) measurement errors of the temperature measuring instruments, and (2) analysis errors in the derived products related to re-mapping of the irregularly sampled temperature observations onto a uniform grid. To estimate the measurement error, we consider a typical measurement accuracy of $0.002\,^{\circ}$ C for Argo floats (Wong et al., 2020), which make up the bulk of the available temperature measurements. On average there are 258 Argo floats in the region between the RAPID and OSNAP lines each month (estimated based on the Argo data in the region between 2014 and 2018). Assuming a $0.002\,^{\circ}$ C error for each Argo float over the domain and summing these errors in quadrature leads to an uncertainty in the OHC estimate for a given month of $4.1\,\times\,10^{19}J$. This is a conservative estimate since there are other temperature measurements besides Argo that are included in the analysis products. The analysis error can be estimated from the root-mean-square (RMS) difference between the four gridded products (Fig. B.1). All four products show a generally consistent OHC signal, with a mean RMS difference of $2.9\,\times\,10^{21}J$. Since all of the data products use the same Argo measurements, it is possible that in certain months the estimates could all have a common bias due to a poor sampling distribution, and therefore we double this uncertainty estimate to $5.8\,\times\,10^{21}\,J$ to account for the uneven sampling distributions. This error dominates the measurement uncertainty in the monthly OHC estimates, and leads to an uncertainty in Q_{OHC} of Q_{OHC}

Similarly, we use four gridded salinity products for deriving FW_{OSC} over the North Atlantic basin between the OSNAP and RAPID lines. This is obtained based on the monthly OSC estimates for the first and last months of a given observation period, following Eq. (8). We consider first the

uncertainty caused by a typical measurement accuracy of 0.01 for salinity from Argo floats (Wong et al., 2020). When assuming this error for all the Argo floats within the domain for any month, it results in an uncertainty in the monthly OSC estimates of $5.1 \times 10^{13} m^3$. We then estimate analysis uncertainty in the monthly OSC estimates related to the mapping procedures and sampling distributions, based on the RMS differences of the four products (Fig. B.2). All data products again show consistent OSC changes, with a mean RMS error of $1.3 \times 10^{14} m^3$. We double this value to account for additional errors due to the sampling distributions, which becomes $2.6 \times 10^{14} m^3$ and dominates the measurement uncertainty in the monthly OSC estimates. This leads to an uncertainty in FW_{OSC} of 0.09 Sv for 8/2014–5/2018, and 0.02 Sv for 2/2004–8/2018 (Table B.2).

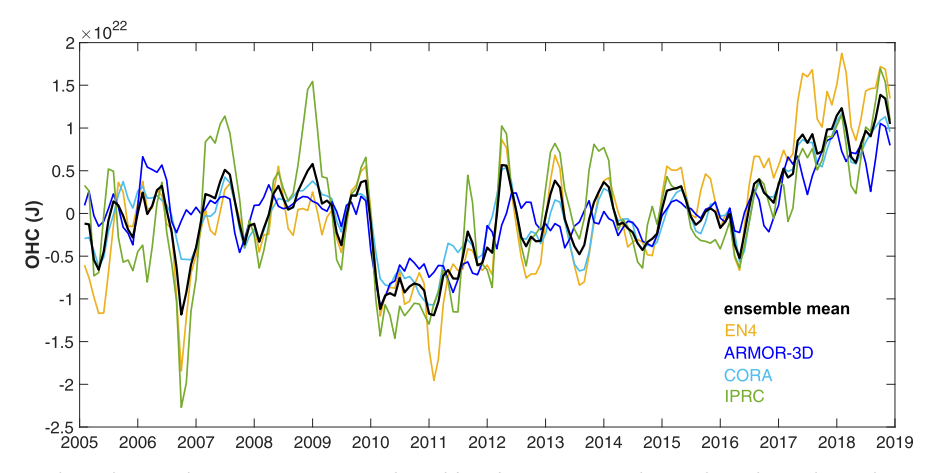


Fig. B1. Monthly OHC anomalies (relative to the respective time mean) derived from four temperature data products, during the overlapping 2005–2018 period. The ensemble means are obtained based on the individual monthly estimates, with the shading for the RMS differences. The seasonal cycles have been removed from each data.

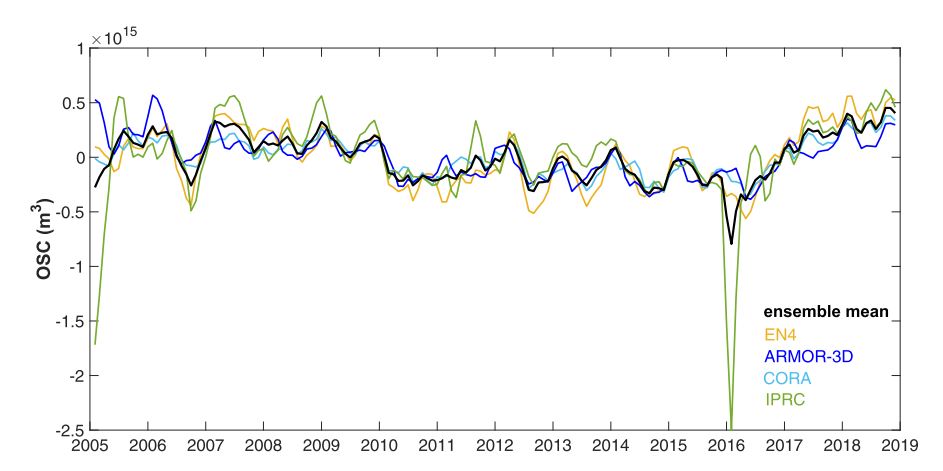


Fig. B2. Monthly OSC anomalies (relative to the respective time mean) derived from four salinity data products, during the overlapping 2005–2018 period. The ensemble means are obtained based on the individual monthly estimates, with the shading for the RMS differences.

 Table B1

 Q_{OHC} derived from the OHC changes at the first and last months during the respective observation period (units: PW). Positive values indicate heat sources for the basin enclosed by the OSNAP and RAPID sections.

| | EN4 | ARMOR-3D | CORA | IPRC | Ensemble-mean \pm uncertainty |
|-----------------|-------|----------|-------|--------|---------------------------------|
| 08/2014-05/2018 | 0.116 | 0.081 | 0.087 | 0.101 | 0.10 ± 0.07 |
| 02/2004-08/2018 | 0.045 | 0.024 | 0.023 | 0.023* | 0.03 ± 0.02 |

^{*} IPRC are only available from 2005 Jan, so the change is for 2005–2018.

Table B2FW_{OSC} derived from the OSC changes at the first and last months during the respective observation period (units: Sv). Negative values indicate freshwater sinks for the ocean basin enclosed by the OSNAP and RAPID sections.

| | EN4 | ARMOR-3D | CORA | IPRC | Ensemble-mean ± uncertainty |
|-----------------|--------|----------|--------|---------|-----------------------------|
| 08/2014-05/2018 | -0.184 | -0.100 | -0.137 | -0.166 | -0.15 ± 0.09 |
| 02/2004-08/2018 | -0.026 | -0.005 | -0.018 | -0.148* | -0.05 ± 0.02 |

^{*} IPRC are only available from 2005 Jan, so the change is for 2005–2018.

Appendix C. Supplementary material

Supplementary data to this article can be found online at https://doi.org/10.1016/j.pocean.2021.102640.

References

- Aagaard, K., Carmack, E.C., 1989. The role of sea ice and other fresh-water in the arctic circulation. J. Geophys. Res.-Oceans 94, 14485–14498.
- Bacon, S., Aksenov, Y., Fawcett, S., Madec, G., 2015. Arctic mass, freshwater and heat fluxes: methods and modelled seasonal variability. Philos. T. R. Soc. A 373.
- Bacon, S., Marshall, A., Holliday, N.P., Aksenov, Y., Dye, S.R., 2014. Seasonal variability of the East Greenland Coastal Current. J. Geophys. Res.-Oceans 119, 3967–3987.
- Bakker, P., Coauthors, 2016. Fate of the Atlantic Meridional Overturning Circulation: Strong decline under continued warming and Greenland melting. Geophys. Res. Lett., 43, 12252-12260.
- Böning, C.W., Behrens, E., Biastoch, A., Getzlaff, K., Bamber, J.L., 2016. Emerging impact of Greenland meltwater on deepwater formation in the North Atlantic Ocean. Nat. Geosci. 9, 523–527.
- Bryden, H.L., Johns, W.E., King, B.A., McCarthy, G., McDonagh, E.L., Moat, B., Smeed, D. A., 2020. Reduction in ocean heat transport at 26 degrees N since 2008 Cools the Eastern Subpolar Gyre of the North Atlantic Ocean. J. Clim. 33, 1677–1689.
- Carmack, E., Coauthors, 2015. Toward quantifying the increasing role of oceanic heat in sea ice loss in the New Arctic. B Am. Meteorol. Soc., 96, 2079-2105.
- Chafik, L., Rossby, T., 2019. Volume, heat, and freshwater divergences in the subpolar North Atlantic suggest the nordic seas as key to the state of the meridional overturning circulation. Geophys. Res. Lett. 46, 4799–4808.
- Cheng, L., Abraham, J., Hausfather, Z., Trenberth, K.E., 2019. How fast are the oceans warming? Science 363, 128–129.
- Cheng, L., Trenberth, K.E., Fasullo, J., Boyer, T., Abraham, J., Zhu, J., 2017. Improved estimates of ocean heat content from 1960 to 2015. Sci. Adv., 3, e1601545e1601545
- Criado-Aldeanueva, F., Soto-Navarro, F.J., Garcia-Lafuente, J., 2012. Seasonal and interannual variability of surface heat and freshwater fluxes in the Mediterranean Sea: budgets and exchange through the Strait of Gibraltar. Int. J. Climatol. 32, 286–302
- Cronin, M.F., Coauthors, 2019. Air-sea fluxes with a focus on heat and momentum. Front. Mar. Sci., 6.
- Cunningham, S.A., Coauthors, 2007. Temporal variability of the Atlantic meridional overturning circulation at 26.5° N. Science, 317, 935-938.
- Curry, B., Lee, C., Petrie, B., 2011. Volume, freshwater, and heat fluxes through davis strait, 2004–05. J. Phys. Oceanography - J PHYS OCEANOGR 41, 429–436.
- Curry, B., Lee, C.M., Petrie, B., Moritz, R.E., Kwok, R., 2014. Multiyear volume, liquid freshwater, and sea ice transports through Davis strait, 2004–10*. J. Phys. Oceanogr. 44, 1244–1266.
- de Steur, L., Peralta-Ferriz, C., Pavlova, O., 2018: Freshwater export in the east Greenland current freshens the North Atlantic. Geophys. Res. Lett., 45, 13,359-313,366.
- Delworth, T.L., Zeng, F., 2016. The impact of the North Atlantic oscillation on climate through its influence on the Atlantic meridional overturning circulation. J. Clim. 29, 941–962.
- Desbruyeres, D.G., Mercier, H., Maze, G., Daniault, N., 2019. Surface predictor of overturning circulation and heat content change in the subpolar North Atlantic. Ocean Sci. 15, 809–817.
- Deser, C., Alexander, M.A., Xie, S.P., Phillips, A.S., 2010. Sea surface temperature variability: patterns and mechanisms. Ann. Rev. Mar. Sci. 2, 115–143.
- Foukal, N.P., Gelderloos, R., Pickart, R.S., 2020. A continuous pathway for fresh water along the East Greenland shelf. Sci. Adv. 6, eabc4254.
- Fu, Y., Karstensen, J., Brandt, P., 2018. Atlantic meridional overturning circulation at 14.5° N in 1989 and 2013 and 24.5° N in 1992 and 2015: volume, heat, and freshwater transports. Ocean Sci. 14, 589–616.
- Fu, Y., Li, F., Karstensen, J., Wang, C., 2020. stable Atlantic Meridional Overturning Circulation in a changing North Atlantic Ocean since the 1990s. Science Advances 6 (48), eabc7836.
- Gaillard, F., Reynaud, T., Thierry, V., Kolodziejczyk, N., von Schuckmann, K., 2016. In situ-based reanalysis of the global ocean temperature and salinity with ISAS: Variability of the heat content and steric height, J. Clim. 29, 1305–1323.
- Ganachaud, A., Wunsch, C., 2000. Improved estimates of global ocean circulation, heat transport and mixing from hydrographic data. Nature 408, 453–457.

- Ganachaud, A., Wunsch, C., 2003. Large-scale ocean heat and freshwater transports during the World Ocean Circulation Experiment. J. Clim. 16, 696–705.
- Good, S.A., Martin, M.J., Rayner, N.A., 2013. EN4: Quality controlled ocean temperature and salinity profiles and monthly objective analyses with uncertainty estimates. J. Geophys. Res.-Oceans 118, 6704–6716.
- Grist, J.P., Josey, S.A., Marsh, R., Kwon, Y.O., Bingham, R.J., Blaker, A.T., 2014. The surface-forced overturning of the North Atlantic: Estimates from Modern Era Atmospheric Reanalysis Datasets. J. Clim. 27, 3596–3618.
- Guinehut, S., Dhomps, A.L., Larnicol, G., Le Traon, P.Y., 2012. High resolution 3-D temperature and salinity fields derived from in situ and satellite observations. Ocean Sci. 8. 845–857.
- Haine, T.W.N., Coauthors, 2015. Arctic freshwater export: Status, mechanisms, and prospects. Global Planet Change, 125, 13-35.
- Han, G.Q., Ma, Z.M., Chen, N., 2019. Ocean climate variability off Newfoundland and
- Labrador over 1979–2010: A modelling approach. Ocean Model. 144.
 Han, G.Q., Lu, Z.S., Wang, Z.L., Helbig, J., Chen, N., de Young, B., 2008. Seasonal variability of the labrador current and shelf circulation off Newfoundland.
 J. Geophys. Res.-Oceans 113.
- Harada, Y., Coauthors, 2016. The JRA-55 reanalysis: Representation of atmospheric circulation and climate variability. J. Meteorol. Soc. Jpn., 94, 269-302.
- Haskins, R.K., Oliver, K.I.C., Jackson, L.C., Wood, R.A., Drijfhout, S.S., 2020.
 Temperature domination of AMOC weakening due to freshwater hosing in two GCMs. Clim. Dyn. 54, 273–286.
- Holland, D.M., Thomas, R.H., De Young, B., Ribergaard, M.H., Lyberth, B., 2008. Acceleration of Jakobshavn Isbrae triggered by warm subsurface ocean waters. Nat. Geosci. 1, 659–664.
- Holliday, N.P., Coauthors, 2018. Subpolar North Atlantic overturning and gyre-scale circulation in the summers of 2014 and 2016. J. Geophys. Res.-Oceans, 123, 4538-4559.
- Holliday, N.P., Coauthors, 2020. Ocean circulation causes the largest freshening event for 120 years in eastern subpolar North Atlantic. Nat. Commun., 11, 585.
- Holte, J., Straneo, F., 2017. Seasonal overturning of the Labrador Sea as observed by arge floats. J. Phys. Oceanogr. 47, 2531–2543.
- IOC, SCOR, and IAPSO, 2010: The international thermodynamic equation of seawater -2010: Calculation and use of thermodynamic properties. Intergovernmental Oceanographic Commission, 196pp pp.
- Jackson, L.C., 2013. Shutdown and recovery of the AMOC in a coupled global climate model: The role of the advective feedback. Geophys. Res. Lett. 40, 1182–1188.
- Johns, W.E., Coauthors, 2011. Continuous, array-based estimates of Atlantic Ocean heat transport at 26.5°N. J. Climate, 24, 2429-2449.
- Josey, S.A., 2001. A comparison of ECMWF, NCEP-NCAR, and SOC surface heat fluxes with moored buoy measurements in the subduction region of the Northeast Atlantic. J. Clim. 14, 1780–1789.
- Josey, S.A., Hirschi, J.J.M., Sinha, B., Duchez, A., Grist, J.P., Marsh, R., 2018. The recent Atlantic cold anomaly: causes, consequences, and related phenomena. Ann. Rev. Mar. Sci. 10 (10), 475–501.
- Kelly, K.A., Thompson, L., Lyman, J., 2014. The coherence and impact of meridional heat transport anomalies in the Atlantic Ocean inferred from observations. J. Clim. 27, 1460–1487
- Kelly, K.A., Drushka, K., Thompson, L., Le Bars, D., McDonagh, E.L., 2016. Impact of slowdown of Atlantic overturning circulation on heat and freshwater transports. Geophys. Res. Lett. 43, 7625–7631.
- Kobayashi, S., Coauthors, 2015. The JRA-55 reanalysis: General specifications and basic characteristics. J. Meteorol. Soc. Jpn., 93, 5-48.
 Le Bras, I.A.A., Straneo, F., Holte, J., Holliday, N.P., 2018. Seasonality of freshwater in
- Le Bras, I.A.A., Straneo, F., Holte, J., Holliday, N.P., 2018. Seasonality of freshwater in the East Greenland current system from 2014 to 2016. J. Geophys. Res.-Oceans 123, 8828–8848.
- Li, F., Lozier, M.S., Johns, W.E., 2017. Calculating the meridional volume, heat, and freshwater transports from an observing system in the subpolar North Atlantic: Observing System Simulation Experiment. J. Atmos. Oceanic Technol. 34, 1483–1500.
- Li, F., Coauthors, 2021. Subpolar North Atlantic western boundary density anomalies and the meridional overturning circulation. Nat. Commun., 12, 3002.

- Liu, W., Liu, Z., 2012. A diagnostic indicator of the stability of the atlantic meridional overturning circulation in CCSM3. J. Clim. 26, 1926–1938.
- Lozier, M.S., Coauthors, 2017. Overturning in the Subpolar North Atlantic Program: A new international ocean observing system. B Am. Meteorol. Soc., 98, 737-752. Lozier, M.S., Coauthors, 2019. A sea change in our view of overturning in the subpolar
- North Atlantic. Science, 363, 516-521.
- Lynch-Stieglitz, J., 2017. The Atlantic meridional overturning circulation and abrupt climate change. Ann. Rev. Mar. Sci. 9, 83–104.
- McCarthy, G.D., Coauthors, 2015. Measuring the Atlantic meridional overturning
- circulation at 26° N. Prog. Oceanography, 130, 91-111. McDonagh, E.L., Coauthors, 2015. Continuous estimate of Atlantic Oceanic freshwater flux at 26.5°N. J. Climate, 28, 8888-8906.
- McDougall, T.J., Barker, P.M., 2011. Getting started with TEOS-10 and the Gibbs seawater (GSW) oceanographic toolbox. SCOR/IAPSO WG127.
- Menary, M.B., Hodson, D.L.R., Robson, J.I., Sutton, R.T., Wood, R.A., 2015. A mechanism of internal decadal Atlantic Ocean variability in a high-resolution coupled climate model. J. Clim. 28, 7764–7785.
- Mercier, H., Coauthors, 2015. Variability of the meridional overturning circulation at the Greenland-Portugal OVIDE section from 1993 to 2010. Prog. Oceanography, 132, 250-261.
- Mertz, G., Narayanan, S., Helbig, J., 1993. The freshwater transport of the labrador current. Atmos. Ocean 31, 281-295.
- Mignac, D., Ferreira, D., Haines, K., 2019. Decoupled freshwater transport and eridional overturning in the South Atlantic. Geophys. Res. Lett. 46,
- Moat, B., Coauthors, 2020. Pending recovery in the strength of the meridional overturning circulation at 26 degrees N. Ocean Sci., 16, 863-874.
- Mulet, S., Rio, M.H., Mignot, A., Guinehut, S., Morrow, R., 2012. A new estimate of the global 3D geostrophic ocean circulation based on satellite data and in-situ measurements. Deep-Sea Res. Pt. Ii. 77–80, 70–81.
- Ortega, P., Mignot, J., Swingedouw, D., Sévellec, F., Guilyardi, E., 2015. Reconciling two alternative mechanisms behind bi-decadal variability in the North Atlantic, Prog Oceanogr. 137, 237–249.
- Østerhus, S., Coauthors, 2019. Arctic Mediterranean exchanges: a consistent volume budget and trends in transports from two decades of observations. Ocean Sci., 15,
- Pacini, A., Coauthors, 2020. Mean conditions and seasonality of the West Greenland Boundary Current System near Cape Farewell. J. Phys. Oceanography, 1-61. Pickart, R.S., Spall, M.A., 2007. Impact of Labrador Sea convection on the North Atlantic
- eridional overturning circulation. J. Phys. Oceanogr. 37, 2207–2227.
- Polyakov, I.V., Coauthors, 2017. Greater role for Atlantic inflows on sea-ice loss in the Eurasian Basin of the Arctic Ocean. Science, 356, 285.
- Polyakov, I.V., Coauthors, 2010. Arctic Ocean warming contributes to reduced polar ice
- cap. J. Phys. Oceanography, 40, 2743-2756.

 Rainsley, E., Menviel, L., Fogwill, C.J., Turney, C.S.M., Hughes, A.L.C., Rood, D.H., 2018.

 Greenland ice mass loss during the Younger Dryas driven by Atlantic Meridional
- overturning circulation feedbacks. Sci. Rep. 8.
 Rhein, M., Coauthors, 2014. Observations: Ocean Pages. Climate Change 2013 The Physical Science Basis: Working Group I Contribution to the Fifth Assessment Report of the Intergovernmental Panel on Climate Change, C. Intergovernmental Panel on Climate, Ed., Cambridge University Press, 255-316.
- Robson, J., Ortega, P., Sutton, R., 2016. A reversal of climatic trends in the North Atlantic since 2005. Nat. Geosci. 9, 513–517. Rogerson, M., Rohling, E.J., Bigg, G.R., Ramirez, J., 2012. Paleoceanography of the
- Atlantic-Mediterranean exchange: overview and first quantitative assessment of climatic forcing. Rev. Geophys. 50. Rossby, T., Reverdin, G., Chafik, L., Søiland, H., 2017. A direct estimate of poleward
- volume, heat, and freshwater fluxes at 59.5°N between Greenland and Scotland. J. Geophys. Res.-Oceans 122, 5870-5887.
- Rossby, T., Flagg, C., Chafik, L., Harden, B., Soiland, H., 2018. A direct estimate of volume, heat, and freshwater exchange across the Greenland-Iceland-Faroe-Scotland Ridge, J. Geophys. Res.-Oceans 123, 7139-7153.
- Saha, S., Coauthors, 2014. The NCEP climate forecast system version 2. J. Climate, 27,
- Sanchez-Roman, A., Sannino, G., Garcia-Lafuente, J., Carillo, A., Criado-Aldeanueva, F., 2009. Transport estimates at the western section of the Strait of Gibraltar: A combined experimental and numerical modeling study. J. Geophys. Res.-Oceans
- Schauer, U., Beszczynska-Moller, A., 2009. Problems with estimation and interpretation of oceanic heat transport - conceptual remarks for the case of Fram Strait in the Arctic Ocean. Ocean Sci. 5, 487–494. Schauer, U., Losch, M., 2019. "Freshwater" in the ocean is not a useful parameter in
- climate research. J. Phys. Oceanogr. 49, 2309-2321.

- Segtnan, O.H., Furevik, T., Jenkins, A.D., 2011. Heat and freshwater budgets of the Nordic seas computed from atmospheric reanalysis and ocean observations J. Geophys. Res.-Oceans 116.
- Skagseth, \emptyset ., Furevik, T., Ingvaldsen, R., Loeng, H., Mork, K.A., Orvik, K.A., Ozhigin, V., 2008. Volume and Heat Transports to the Arctic Ocean Via the Norwegian and Barents Seas. In: Dickson, R.R., Meincke, J., Rhines, P. (Eds.), Arctic-Subarctic Ocean Fluxes: Defining the Role of the Northern Seas in Climate. Springer, Netherlands,
- Smedsrud, L.H., Ingvaldsen, R., Nilsen, J.E.Ø., Skagseth, Ø., 2010. Heat in the Barents Sea: transport, storage, and surface fluxes. Ocean Sci. 6, 219–234. Soto-Navarro, J., Criado-Aldeanueva, F., Garcia-Lafuente, J., 2010. Estimation of the
- Atlantic inflow through the Strait of Gibraltar from climatological and in situ data. J. Geophys. Res.-Oceans 115.
- Straneo, F., 2006. Heat and freshwater transport through the central Labrador Sea*. J. Phys. Oceanogr. 36, 606-628.
- Straneo, F., Heimbach, P., 2013. North Atlantic warming and the retreat of Greenland's outlet glaciers. Nature 504, 36–43.
- Sutton, R.T., McCarthy, G.D., Robson, J., Sinha, B., Archibald, A.T., Gray, L.J., 2018. Atlantic multidecadal variability and the UK ACSIS program. B Am. Meteorol. Soc. 99, 415-425,
- Thomson, R.E., Emery, W.J., 2014. Time-series Analysis Methods. Data Analysis Methods in Physical Oceanography, 3 ed., R. E. Thomson, and W. J. Emery, Eds., Elsevier Science, 284.
- Trenberth, K.E., Caron, J.M., 2001. Estimates of meridional atmosphere and ocean heat transports, J. Clim. 14, 3433-3443.
- Trenberth, K.E., Fasullo, J.T., 2017. Atlantic meridional heat transports computed from balancing Earth's energy locally. Geophys. Res. Lett. 44, 1919-1927.
- Trenberth, K.E., Caron, J.M., Stepaniak, D.P., 2001. The atmospheric energy budget and implications for surface fluxes and ocean heat transports. Clim. Dyn. 17, 259–276.
- Trenberth, K.E., Zhang, Y.X., Fasullo, J.T., Cheng, L.J., 2019. Observation-based estimates of global and basin ocean meridional heat transport time series. J. Clim.
- Tsubouchi, T., Coauthors, 2021. Increased ocean heat transport into the Nordic Seas and
- Arctic Ocean over the period 1993–2016. Nat. Climate Change, 21-26. Tsubouchi, T., Coauthors, 2018. The Arctic ocean seasonal cycles of heat and freshwater fluxes: observation-based inverse estimates. J. Phys. Oceanography, 48, 2029-2055.
- Tsubouchi, T., Coauthors, 2012. The Arctic Ocean in summer: A quasi-synoptic inverse estimate of boundary fluxes and water mass transformation. J. Geophys. Res.
- C3S (C.C.C.S.), 2017: ERA5: Fifth generation of ECMWF atmospheric reanalyses of the global climate. Copernicus Climate Change Service Climate Data Store (CDS).
- Valdivieso, M., Coauthors, 2017. An assessment of air-sea heat fluxes from ocean and coupled reanalyses. Climate Dyn., 49, 983-1008. Wang, Q., Ilicak, M., Gerdes, R., Drange, H., Aksenov, Y., Bailey, D.A., Bentsen, M.,
- Biastoch, A., Bozec, A., Böning, C., Cassou, C., Chassignet, E., Coward, A.C., Curry, B., Danabasoglu, G., Danilov, S., Fernandez, E., Fogli, P.G., Fujii, Y., Griffies, S.M., Iovino, D., Jahn, A., Jung, T., Large, W.G., Lee, C., Lique, C., Lu, J., Masina, S., Nurser, A.J.G., Rabe, B., Roth, C., Mélia, D.S., Samuel, B.L., Spence, P., Tsujino, H., Valcke, S., Voldoire, A., Wang, X., Yeager, S.G., 2016. An assessment of the Arctic Ocean in a suite of interannual CORE-II simulations. Part II: Liquid freshwater. Ocean Modelling 99, 86-109. https://doi.org/10.1016/j ocemod.2015.12.009.
 Wang, Z.L., Yashayaev, I., Greenan, B., 2015. Seasonality of the inshore Labrador current
- over the Newfoundland shelf. Cont. Shelf Res. 100, 1-10.
- Weijer, W., Maltrud, M.E., Hecht, M.W., Dijkstra, H.A., Kliphuis, M.A., 2012. Response of the Atlantic Ocean circulation to Greenland Ice Sheet melting in a strongly-eddying ocean model. Geophys. Res. Lett. 39
- Weijer, W., Coauthors, 2019. Stability of the Atlantic meridional overturning circulation: a review and synthesis. J. Geophys. Res.-Oceans, 124, 5336-5375.
- Wong, A.P.S., Coauthors, 2020. Argo data 1999–2019: Two million temperature-salinity profiles and subsurface velocity observations from a global array of profiling floats. Front. Mar. Sci., 7, 700.
- Woodgate, R.A., 2018. Increases in the Pacific inflow to the Arctic from 1990 to 2015, and insights into seasonal trends and driving mechanisms from year-round Bering Strait mooring data. Prog. Oceanogr. 160, 124–154.
- Yang, Q., Dixon, T.H., Myers, P.G., Bonin, J., Chambers, D., van den Broeke, M.R., 2016. Recent increases in Arctic freshwater flux affects Labrador Sea convection and Atlantic overturning circulation. Nat. Commun. 7.
- Yu, L.S., 2019. Global air-sea fluxes of heat, fresh water, and momentum: energy budget closure and unanswered questions. Ann. Rev. Mar. Sci. 11 (11), 227–248. Zanna, L., Khatiwala, S., Gregory, J.M., Ison, J., Heimbach, P., 2019. Global
- reconstruction of historical ocean heat storage and transport. Proc. Natl. Acad. Sci. 116, 1126-1131.